LEGIBILITY NOTICE

A major purpose of the Technical Information Center is to provide the broadest dissemination possible of information contained in DOE's Research and Development Reports to business, industry, the academic community, and federal, state and local governments.

Although a small portion of this report is not reproducible, it is being made available to expedite the availability of information on the research discussed herein.

LA-UR- 87-3261 CONF-8708141--2

Los Alamos National Laboratory is operated by the University of California for the United States Department of Energy under contract W-7405-ENG-36

LA-UR--87-3261

DE88 000483

TITLE: Slow-Mode Shocks in the Earth's Magnetosphere

AUTHOR(S): William C. Feldman

SUBMITTED TO: Proceedings of Solar Wind 6 Conference, Estes Park, CO, August 1987

DISCLAIMER

Los Alamos National Laboratory
Los Alamos, New Mexico 87545

Slow-Mode Shocks in the Earth's Magnetosphere

by

William C. Feldman

Los Alamos National Laboratory, Mail Stop D438, Los Alamos, NM 87545

Abstract

The locations and structure of slow-mode shocks in the earth's magnetosphere are reviewed. To date, such shocks have only been identified along the high latitude portions of the lobe-plasma sheet boundary of the geomagnetic tail. Although their intrinsic thickness is of the order of the upstream ion inertial length, they affect the internal state of a relatively much larger volume of surrounding plasma. In particular, they support a well-developed foreshock very similar to that observed upstream of the earth's bow shock, and a turbulent, strongly convecting downstream flow. They also figure importantly in the energy budget of geomagnetic substorms and produce effects which are closely analogous to much of the phenomenology known from solar observations to be associated with two-ribbon flares.

1) Introduction

Slow mode shocks are one of five possible MHD discontinuities (Colburn and Sonett, 1966) supported by dilute plasmas. They are steepened, "supersonic," dissipating waves across which magnetic energy in the form of a Poynting flux, is transformed into plasma energy in the form of a kinetic bulk convection flux, an enthalpy flux, and a heat flux. Their relative importance in space and astrophysical plasmas, stems from their direct effect on the bulk characteristics of the plasmas and magnetic fields which cross them and their indirect effect on the structure of a large volume of neighboring upstream plasma. They may also accelerate a few particles to relatively high energies.

There are several locations in the terrestrial magnetosphere where slow shocks may occur. Consider first the magnetopause. An early analysis of the structure of the magnetosphere (Levy *et al.*, 1964) suggested that the boundary layer behind the magnetopause near its sunward edge may, at times, be a slow-mode expansion fan. This fan could extend (at times of steady upstream conditions), from near the nose of the magnetosphere to its flanks well behind the cusps. Such a configuration was drawn schematically by Levy *et al.* (1964) and is shown in Fig. 1. A slow expansion fan may also occur in more localized geometries

throughout the entire magnetopause boundary layer depending on the magnetic field orientation in the upstream flow (e.g., Gosling *et al.*, 1986, and references therein).

The foregoing, slow expansion fan substructure of the magnetopause was predicted by Levy *et al.* (1964) under the assumption that the front-side magnetosphere is a vacuum. As such it could never steepen to form a slow-mode shock. However, if the ring-current density is ever high enough, an additional inward propagating slow-mode compressive fan may form on the earthward side of the slow-mode expansion fan. This component of the inner magnetopause would then stand in the outward-flowing ring-current ions and deflect them to the sides. If conditions allow, the leading edge of this hypothetical, innermost fan, may steepen into a slow-mode shock. Such a structure could also exist at high latitudes tailward of the cusps during periods of northward magnetic field (e.g., see field topology sketched in Dungey, 1961). To date, however, no such shock has been identified anywhere within the magnetopause boundary layer.

Another possible site for slow-mode shocks within the earth's magnetosphere is at the leading edge of plasmoids accelerated tailward into the pre-existing plasma sheet during the expansion phase of geomagnetic substorms . This possibility follows from the theory of time-dependent reconnection (Pudovken and Semenov, 1985, and references therein). However, it appears unlikely in the geomagnetic tail. Slow-mode waves would likely dampen before they steepen into shock waves in the plasma sheet of the distant geomagnetic tail because the ratio of plasma pressure to magnetic pressure there is greater than one (see e.g., analysis in Hada and Kennel, 1985). Indeed, this fact may be the reason why slow-mode shocks have not yet been identified near the leading edges of plasmoids observed in the distant geomagnetic tail (Feldman *et al.*, 1985).

A last possible site for the occurrence of slow-mode shocks occurs along the high-latitude, lobe-plasma-sheet boundaries in the geomagnetic tail. This possibility was first suggested by Levy *et al.* (1964) in accordance with the model of magnetic field reconnection proposed by Petchek (1964). Slow-mode shocks which fit this model have been identified recently (Feldman *et al.*, 1984a; Smith *et al.*, 1984). The rest of this review will be devoted to presenting the observational evidence that support their existence and that detail their role in determining the structure and dynamics of the central portion of the geomagnetic tail.

Evidence to support the existence of slow-mode shocks bounding the geotail plasma sheet will be presented first in Section 2 followed by their influence on neighboring plasmas in Section 3. The development of section 3 will draw heavily on analogy with the earth's bow shock and foreshock. The internal structure

of these shocks will be detailed next in Section 4, and their role in geomagnetic substorms is given in Section 5. Section 6 will summarize all observations in terms of the presently, most widely accepted paradigm of magnetotail structure. This paradigm will then be compared with a similar one used often to organize a large body of observations of two-ribbon solar flares.

2) Existence of Slow Shocks in the Geomagnetic Tail

The north and south bounding surfaces of the plasma sheet in the distant geomagnetic tail were first recognized as slow-mode shocks using plasma and magnetic field data measured aboard ISEE 3 (Feldman *et al.*, 1984; Smith *et al.*, 1984). A qualitative overview of the data record from the first passage of ISEE 3 through the deep geotail revealed sharp transitions marking the boundary between the lobe and the plasma sheet, having all the correlated changes required of a slow-mode shock. Traversal of the boundary from the plasma sheet to the lobe is accompanied by an increase in the magnitude of the magnetic field, B, and decreases in the plasma number density, N, the electron temperature T_e (proton temperatures were not measured aboard ISEE 3 due to a failure in the ion plasma analyzer), and the tailward-directed component of the plasma bulk velocity, $-V_x$.

A schematic view of the reconnection topology in the distant geomagnetic tail which organizes much of the ISEE 3 data is shown in Fig. 2. The diagram at the bottom shows a coordinate system appropriate for an analysis of that part of the southern plasma sheet boundary encircled at the lower right in the top view. A crossing at such a location was observed at 2213 UT on 23 March 1983 at $X = -119$ R_E. Selected electron velocity moments and magnetic field components (in GSE coordinates) are shown in Fig. 3. The hatched region above the plots of plasma density and magnetic field magnitude delineate the traversal of interest. The southern edge of the plasma sheet crossed at $\sim$ 2215 UT is identified as a slow-mode shock and is identified in the figure by the two solid vertical lines. Evidently a small oscillatory motion of this boundary carried it first north completely across ISEE 3, then south partially touching ISEE 3, and then finally north again leaving ISEE 3 permanently in the south lobe at 2220 UT. Scanning the data from top to bottom, one verifies a decrease in density, flow speed, and electron temperature across the plasma sheet-lobe boundary going from left to right, respectively, at 2213 UT, and an increase in the electron heat flux, Q_e, and magnetic field magnitude. Although small oscillations in the magnetic field azimuth are encountered at 2213 UT, all secular changes in the average azimuth occurred before 2213 UT, where $\hat{B}$ executed a single rotation from 0° (sunward pointing) through 90° (dawnward pointing) to 180° (tailward

pointing). Finally, the polar angle of B swings from a direction strongly southward to near 0° at 2213 UT. Although not shown in Fig. 3, the flow speed, which maximizes near 900 km/s before 2213 UT, is directed tailward ($-\hat{X}$) as indicated in the inset diagram in Fig. 2, and the heat flux is also directed tailward in the lobe after 2213 UT. We note in passing that the heat flux stays high for some time after 2220 UT before dropping by an order of magnitude to background. This precipitous drop is identified as the separatrix and shown in Figs. 2 and 3 as dashed lines.

Another example of a slow-mode shock bounding the deep-tail plasma sheet is reproduced in Fig. 4. Here the crossing occurred at about 220 R_E downstream of the earth. It appears as a single, clean traversal of the distant plasma sheet-south lobe boundary at 1922 UT as indicated by the solid vertical line. Careful inspection of all parameter variations shows the same correlations seen in Fig. 3, qualitatively consistent with that expected for a slow-mode shock. In addition, we note that here, as before, the heat flux remains high in the lobes after traversing the shock at 1922 UT until it traverses the separatrix sometime after 1940 UT, denoted by a dashed vertical line in Fig. 4. A data gap prevents a precise identification of this boundary. Note also that the azimuth of $\overline{B}$ again executes a single rotation from 0° to 180° through 90° in the plasma sheet before the shock is encountered.

Although the foregoing qualitative analysis shows that the bounding surface separating the plasma sheet and lobes in the distant geomagnetic tail is consistent with a slow-mode shock, more information is needed for a definitive identification. In particular, one needs to verify a) that the lobe-plasma sheet boundary is the front of a propagating disturbance, b) that the velocity of this disturbance is supersonic relative to the slow-mode speed yet subsonic relative to the intermediate-mode speed, and c) that the transition from upstream (lobe) to downstream (plasma sheet) is accompanied by sufficient dissipation to increase entropy.

Starting first with (a), we note that any boundary in a MHD fluid must propagate through the fluid if the normal component of $\overline{B}$ relative to the boundary, B_n, is nonzero. This result can be derived from a subset of the one-fluid Rankine-Hugoniot relations. However magnetic connectivity from one volume of plasma to another is most decisively proven using suprathermal test particles. Indeed, this method was first used to prove that the polar regions of the terrestrial magnetosphere were magnetically linked to the sun by observing the direct entry of flare-generated solar energetic particles (see e.g., West and Vampola, 1971; Fennell, 1973). A magnetic linkage from the plasma sheet to both lobes in the distant tail proving

that $B_n \neq 0$ was likewise proven by observing suprathermal plasma-sheet electrons in the lobes where they appear as a tailward-flowing heat flux, and a downstream-directed beam of lobe electrons crossing the boundary into the plasma sheet. Cuts through electron velocity distributions measured parallel to $\overline{B}$ aboard ISEE 3 during the 2 Feb 1983 crossing showing this fact, are reproduced in Fig. 5 (Feldman *et al.*, 1985a). Note that the velocity distribution measured in the southern tail lobe at 1922:45 UT has a net heat flux directed tailward, indicated by the hatched region at negative V_x. An electron beam directed into the plasma sheet is also seen at positive V_x within the boundary transition at 1919:56 UT. This beam is most readily explained as resulting from acceleration toward the plasma sheet by a magnetic field-aligned electric field needed to maintain charge neutrality across a magnetically-open boundary (Feldman *et al.*, 1983; Schwartz *et al.*, 1987).

Proof that the disturbances marking the plasma sheet-lobe boundary surface is propagating at a speed between the slow-mode and intermediate-mode speeds requires solution of the one-fluid Rankine-Hugoniot relations. Such an analysis was completed for 26 events similar to and including those shown in Figs. 3 and 4 (Feldman *et al.*, 1984b; Schwartz *et al.*, 1987). Indeed, all events had slow-mode Mach numbers greater than one, averaging 4.7, yet had intermediate-mode Mach numbers less than one, averaging 0.94.

The last requirement, of sufficient dissipation to increase entropy across the boundary, could only be checked partially using the present data set. A sufficient condition for proof of such an increase is if

$$1.5\,\ell n\,(T_d/T_u) > \ell n\,(N_d/N_u) \tag{1}$$

where subscripts u and d denote upstream and downstream parameter values, respectively (Smith *et al.*, 1984). Unfortunately, only electron temperatures were available for the ISEE-3 distant-tail crossings. Since $T = T_e + T_p$, and the Rankine-Hugoniot analyses generally require $T_d/T_u > T_{ed}/T_{eu}$, a check for the validity of the inequality in equation (1) using the electron temperature alone should provide a lower-limit check on the existence of sufficient dissipation. Nevertheless, application of equation 1 to all the parameters listed in Table 1 of Schwartz *et al.* (1987) shows that 21 of the 26 transitions identified as slow-mode shocks showed sufficient dissipation in the electrons alone to ensure that the downstream entropy was greater than that upstream. Four of the five transitions that did not satisfy equation 1 were sufficiently close as to leave little doubt that the ions could have accounted for the deficit, and one transition is presently uncertain.

We therefore conclude that the boundary between the plasma sheet and the lobe in the distant geomagnetic tail is often a slow-mode shock. To date only one boundary crossing in the near geomagnetic

tail has been checked sufficiently quantitatively (Feldman *et al.*, 1987) to prove that, at times, slow-mode shocks may form the leading edge of these boundaries as well.

3) Slow-Mode Foreshocks

A relatively thin boundary layer, separating the plasma sheet and lobes, has been identified recently as a distinct, enduring feature of the geomagnetic tail (Lui *et al.*, 1977, 1983; Decoster and Frank, 1979; Parks *et al.*, 1979, 1984; Möbius *et al.*, 1980; Forbes *et al.*, 1981; Frank *et al.*, 1981; Andrews *et al.*, 1981; Sharp *et al.*, 1981, 1982; Spjeldvik and Fritz, 1981; Williams, 1981; Cowley *et al.*, 1984; Orsini *et al.*, 1984; Eastman *et al.*, 1984, 1985; Scholer *et al.*, 1984; Richardson *et al.*, 1984; Pederson *et al.*, 1985). Two schematic views of this layer in relation to neighboring structures, thought to exist often in the geomagnetic tail, are shown in Fig. 6. Whereas the top view shows a cut along the noon-midnight meridian, the bottom view shows a cut parallel to the dawn-dusk meridian through the tail looking earthward.

Average measured properties of these layers, on either the earthward or tailward side of the neutral line, differ only slightly. These differences are readily explained by the presence of the ionosphere and a mirror magnetic field geometry on the earthward side, and the interplanetary medium and an open-field geometry on the tailward side. However, their characteristics can change greatly during geomagnetic substorms. Nevertheless, the following general properties are often observed. These can be simply organized by progressing along a direction antiparallel to their outward normal from the lobes into the plasma sheet. Starting first on the earthward side of the neutral line, one first encounters high energy electrons at the separatrix boundary. These electrons are not streaming but may at times have a bidirectional anisotropy (Spjeldvik and Fritz, 1981; Parks *et al.*, 1984). Enhancements in electron fluxes at suprathermal energies are also seen to begin at this boundary (Parks *et al.*, 1984; Feldman *et al.*, 1987). They are observed to have variable but generally field aligned anisotropies. At times these anisotropies are unidirectional in the ion frame of reference yielding field-aligned currents (Frank *et al.*, 1981).

A layer of energetic and suprathermal ions begins inside the outer edge of the boundary layer as defined by the energetic and suprathermal electrons. The highest energy ions occur first and are generally observed to be streaming earthward (Möbius *et al.*, 1980; Andrews *et al.*, 1981; Spjeldvik and Fritz, 1981; Williams, 1981; Lui *et al.*, 1983). At lower energies, these suprathermal ions often appear as a distinct entity convecting earthward through the ambient lobe plasma (Decoster and Frank, 1979). They can also appear as an ion heat flux directed earthward (Feldman *et al.*, 1987). Closer to the plasma sheet, beams of

tailward directed ions are seen superimposed on the earthward beams just mentioned (Forbes *et al.*, 1981; Andrews *et al.*, 1981; Williams, 1981). Streams of tailward-propagating ionospheric oxygen ions as well as counter streaming O^+ beams are sometimes observed to be enhanced during periods of geomagnetic activity (Sharp *et al.*, 1981; Orsini *et al.*, 1984; Eastman *et al.*, 1984).

Although there are some notable exceptions, the structure of the plasma sheet boundary layer tailward of the neutral line is remarkably similar to that earthward of the neutral line. Again, progressing antiparallel to the outward normal of the separatrix boundary surface, a layer of tailward-streaming energetic electrons is encountered first, thereby defining the separatrix boundary surface (Baker and Stone, 1976, 1977; Bieber and Stone, 1980; Bieber *et al.*, 1982; Bieber, 1984; Scholer *et al.*, 1984a). No bidirectional electron fluxes are observed in this layer in contrast to the case earthward of the neutral line. In the suprathermal energy range, a strong, tailward-directed electron heat flux is also observed to start at the separatrix boundary (Feldman *et al.*, 1984a, 1984b, 1985). Further in, but close to the separatrix boundary, a tailward streaming flux of suprathermal ions is encountered next (Cowley *et al.*, 1984; Richardson and Cowley, 1985). In contrast to that observed in the earthward components of the plasma-sheet boundary layer, no return (in this case, earthward-directed) ion fluxes are seen in the distant-tail boundary layer.

A variety of strong wave activity is observed to accompany the foregoing enhanced particle fluxes in the plasma-sheet boundary layers. Near the earth, enhanced levels of broadband electrostatic turbulence are observed near to, but outside of, the plasma sheet (Scarf *et al.*, 1974; Gurnett *et al.*, 1976). Whistler-mode bursts (Gurnett *et al.*, 1976) as well as large electric field spikes (Cattell *et al.*, 1982; Pedersen *et al.*, 1985) are sometimes observed cospatially Enhanced levels of broadband electrostatic turbulence are also observed in the far-tail, plasma-sheet boundary layer (Scarf *et al.*, 1984a). However, additional wave activity observed in the distant tail that has not been reported in the near tail layer are intense fluxes of plasma waves (Scarf *et al.*, 1984b) and tailward propagating magnetosonic waves (Tsurutani and Smith, 1984; Tsurutani *et al.*, 1985).

A pictorial representation summarizing all the foregoing observations is synthesized in Fig. 7. The similarities of this representation with that developed for the earth's foreshock (see, e.g., Thomsen, 1985; Klimas, 1985; and references therein), are seen to be sufficiently close to identify the plasma-sheet boundary layers in the geomagnetic tail as slow-mode foreshocks. The lobes of the geomagnetic tail are then analogous to the bow-shock unperturbed solar wind, and the plasma sheath is analogous to the shocked solar wind,

or magnetosheath.

4) Internal Structure of a Slow-Mode Shock

The only detailed study of the internal structure of a slow-mode shock was conducted recently (Feldman *et al.*, 1987). This shock marked the northern boundary of the near-earth plasma sheet during the recovery phase of an isolated geomagnetic substorm which commenced at 1112 UT on 24 April 1979. A selection of plasma and field parameters detailing this shock transition is shown in Fig. 8. From top to bottom are the magnitude of the magnetic field, B, the electron number density, N_E, the X-component of the proton bulk velocity, V_{xp} (downward going speeds represent earthward flow), and the electron, T_e, and proton, T_p, temperatures. The vertical lines in both temperature plots connect the maximum and minimum values of the diagonalized temperature tensors. No proton data is plotted before about 1140 UT because the density is not sufficiently high to allow a reliable determination of the velocity moments of single measurements of the proton velocity distribution function.

An overview of the parameter variations in Fig. 8 shows the same qualitative trends noted earlier for the slow-mode shocks in the distant tail; B decreases from the lobe (left) to the plasma sheet (right) while N, $|V|$, and T increase. In contrast to the earlier examples, though, the plasma jets toward, rather than away, from the earth and the entire transition here is not a shock. Rather, the relatively small decrease in B at about 1142:30 (located between the third and fourth vertical lines from the left) is the shock and is followed by a large-amplitude, slow-mode compression fan. The fact that the plasma is observed to jet toward the earth downstream of the shock indicates that it represents that part of the plasma sheet boundary earthward of the neutral line.

Our presentation of the internal structure of this slow-mode shock will start on the upstream side (to the left in Fig. 8) and proceed systematically through the shock to the downstream side (to the right in Fig. 8). The first encounter with the shock appears at about 1139 UT as a modest enhancement in the electron temperature and density. This foot-like feature, representing an upstream electron heating that extends to about 1141:20 UT, can be identified with the electron foreshock. Contained within the upstream edge of the electron foreshock is a strong, earthward directed ion heat flux, which starts at about 1140:40 UT and terminates near the upstream edge of the shock as shown in Fig. 9. This feature can be identified with the proton foreshock.

The shock transition itself supports a macroscopic, electrostatic potential gradient. The sign of this

gradient is such as to accelerate the upstream electrons through the shock to the downstream plasma sheet. Its magnitude can be inferred from the energy of the peak of the downstream-directed electron beam at the downstream edge of the shock (Schwartz *et al.*, 1987). This estimate is made here using the last of the four electron velocity distributions measured at times labeled 1 through 4 in Fig. 8 and shown in Fig. 10. The electron beams in the parallel cuts in all four distributions at negative velocities (tailward directed) are clearly evident. The peak of the parallel cut through distribution four occurs at 10.8×10^3 km/s, or equivalently, $\simeq$ 330 eV. This value is close to the average potential drop across the 26 distant-tail slow-mode shocks studied by Schwartz *et al.*, $\langle \Delta\Phi \rangle = 215$ V.

The thickness of the 27 April 1979 show-mode shock was inferred from direct measurements of the current and the magnetic field using

$$\overline{J} = eN\left(\overline{V}_p - \overline{V}_e\right) = \frac{c}{4\pi}\overline{\nabla} \times \overline{B} \tag{2}$$

Thirty-second averages of the X and Y components of the electron and ion bulk velocities are shown in Fig. 11. Careful inspection shows two intervals when V_{xe} differs from V_{xp} by more than two standard deviations and two intervals when V_{ye} differs from V_{yp} by more than two standard deviations. These times mark intervals of electron-ion bulk velocity differences or currents. Proceeding from left (upstream) to right (downstream) in Fig. 11, the first such interval shows a current in the $-$X direction (antiparallel to $\overline{B}$ or directed tailward, away from the ionosphere). Since from Fig. 11 the velocity difference amounts to about 140 km/s and the density from Fig. 8 is 10^{-2} cm^{-3}, this field-aligned current amounts to $J_x \cong -7 \times 10^{-10}$ Amps/m^2. Although this current occupies a location relative to the lobe-plasma sheet boundary similar to that occupied by the ones reported by Frank *et al.* (1981), their relationship is uncertain. The current measured here is more than an order of magnitude less than the ones measured by Frank *et al.* (1981).

Progressing downstream, the next current is cospatial with the region within the shock front where electrons heat. It is directed in the positive y direction or from dawn to dusk. This direction is consistent with that expected for the cross-tail current that supports the slow-mode shock. This current is the one responsible for accelerating the newly entering lobe plasma earthward to form the observed downstream plasma jets. Its magnitude is seen to be $J_y = +2.1 \times 10^{-9}$ A/m^2. Application of equation 2 yields a shock thickness of $\Delta\ell = 2100$ km. This thickness is 3.5 times the downstream ion gyroradius, $\lambda_d = 600$ km, and comparable to the upstream ion inertial length, $c/\omega_{piu} = 1930$ km.

The last current system in Fig. 11 consists of a pair, pointing first in the +X direction and then in the +Y direction. It is shown in the lowest panel of Fig. 11 to be the current system that supports an upstream-directed, trailing ion-cyclotron wave. Such a wave was predicted initially by Coroniti (1971) and later found in computer simulations of slow-mode shocks (Swift, 1983; Winske *et al.*, 1985; Winske, 1987). Application of equation 2 yields a wavelength, $\lambda_m = 2370$ km. This value is close to that expected, λ_w, for the trailing ion-cyclotron wave having k vector along the boundary normal and a phase speed just sufficient to stand in the oncoming flow. Using parameters from a one-fluid Rankine-Hugoniot analysis of the shock transition gives $\lambda_w = 2490\,\mathrm{km} \simeq \lambda_m$.

The fact that the amplitude of this cyclotron wave ($\Delta B_y \sim 5 \times 10^{-5}$ G from the bottom panel of Fig. 11) is comparable to the decrement in B across the shock ($\Delta B \simeq 5 \times 10^{-5}$ G from the top panel of Fig. 8) suggests that the damping of this wave accounts for a significant part of the shock structure. The fact that $\lambda_m \simeq \Delta\ell$ then suggests that the steepness of the 24 April 1979 slow-mode shock is limited by wave dispersion and not anomalous resistivity. If this result applies more generally, it would explain why the measured intensity of broadband electrostatic turbulence observed within the 23 March 1983 and 2 Feb 1983 slow mode shocks in the distant tail was not sufficient to account for their presumed thicknesses, $\sim 3\,c/\omega_{piu}$ (Scarf *et al.*, 1984b). However, trailing ion-cyclotron wave trains have not yet been identified in the ISEE-3, distant-tail data.

5) Role of Slow-Mode Shocks in Substorms

Geomagnetic substorms are the dominant dynamical activity of the terrestrial magnetosphere. They occur sufficiently often relative to their relaxation time as to bring into question whether a quiet magnetospheric state exists. Regardless, though, relatively quiet conditions are observed occasionally so that a steady state appears to be approached. Such a state requires about 2 to 3 hours of settling time. Since the occurrence of slow-mode shocks is intimately associated with magnetic reconnection, which in turn is intimately associated with geomagnetic substorms (e.g., Russell and McPherron, 1973), it is fair to inquire what the relation is between the occurrence of slow-mode shocks and substorms.

This question was addressed using a set of 26 slow-shock events identified in ISEE 3 data measured in the distant geomagnetic tail (Feldman *et al.*, 1985a). Results of this study showed that 13 of these events could not be classified into any one phase of substorm activity because they were occurring too rapidly to allow a unique identification. Nine and possibly ten of the remaining events occurred during the recovery

phase of a substorm, one and perhaps two occurred during the substorm expansion phase, and one and perhaps two occurred during quiet times or perhaps the growth phase of a substorm.

In view of the fact that boundaries in the geomagnetic tail are encountered most often during times of extreme dynamical activity, the fact that slow-mode shocks were found to bound the far-tail plasma sheet most often during active times is not surprising. However, the fact that they were observed during all phases of geomagnetic activity led to the conclusion that these shocks are a semipermanent feature of the distant geomagnetic tail. The intimate relationship between magnetic reconnection and slow-mode shocks (e.g., Petchek, 1964) then implies that oppositely directed north and south lobe magnetic fields are merging nearly all the time but at widely differing rates. When conditions are quiet, the merging rate is slow, and when conditions are active, the merging rate increases to high levels. This suggestion is consistent with a recent update (Hones, 1979) of the paradigm of geomagnetic activity originally developed by Russell and McPherron, 1973). This update is reproduced here in Fig. 12.

During quiet times (Phase 1) magnetic reconnection is occurring at a slow rate in the distant tail near $X \simeq -100$ R_E. When the interplanetary magnetic field carried by the solar wind turns southward, the rate of magnetic reconnection at the magnetopause becomes enhanced and some solar wind energy is transferred to the magnetotail where it is stored temporarily as magnetic energy density in the lobes. The resultant increase in transverse pressure in the lobes compresses the near-Earth plasma sheet until a new neutral line forms, generally between about $X = -10$ R_E and $X = -20$ R_E (Phase 2). Merging then proceeds to sever the part of the plasma sheet lying between the new and old neutral lines forming a disconnected plasmoid (Phases 3 through 5). Upon completion, the plasmoid accelerates tailward driving the old neutral line ahead of it (Phases 6 through 8). Continued reconnection refills that part of the plasma sheet earthward of the near-Earth neutral line building sufficient back pressure to accelerate the near-earth neutral line tailward until it occupies the same location previously occupied by the old neutral line (Phases 9 and 10). Its exact location is fixed by a balance between the rate at which new plasma sheet is created from the lobes and the rate of loss near the Earth due to convection to the front side of the magnetosphere and eventual loss to the front-side magnetosheath through "quiet-time" reconnection. This location appears to lie near $X = -100$ R_E on average (Zwickl *et al.*, 1984).

The initial question concerning the role of slow-mode shocks in substorms can now be rephrased in the context of the foregoing paradigm. We therefore ask instead, about the relative contribution of the

far-tail slow-mode shocks to the energy budget of the magnetotail. This question was addressed using the foregoing 26 events assuming they comprise a representative sample of slow-mode shocks in the distant tail (Feldman *et al.*, 1984b). They had an average merging rate, expressed in terms of the upstream Alfvén Mach number, M_A, amounting to $M_A = 0.19 \pm 0.08$, an average transverse electric field within the shocks of $E_{y'} = 1.6 \pm 0.7$ mV/m, and an average Poynting flux crossing the shocks of $\Delta s = 9.2 \pm 7.4 \times 10^{-3}$ erg/cm^2/s.

Estimation of the total power dissipated across these shocks requires a knowledge of their area. Since 25 of the 26 shock events were measured near $X = -200$ R_E and the neutral line generally lies earthward of $X = -100$ R_E (Zwickl *et al.*, 1984), we estimate a length, $\ell \gtrsim 100$ R_E. Their width, w, follows from the measured value of E'_y, and the average voltage drop measured across the polar cap during periods of moderate geomagnetic activity, $\langle \Delta\Phi \rangle = wE_{y'} = 70$ keV (Reiff *et al.*, 1981). Assuming $E_{y'}$ is constant along the neutral line, we estimate $w \cong 7$ R_E. Putting everything together, we find the average power dissipated tailward of the neutral line from lobe magnetic energy density in the form of a Poynting flux, to plasma energy density in the plasma sheet in the form of bulk convection flux, convected enthalpy, and heat flux, amounts to $\langle U_s \rangle \cong 5 \times 10^{18}$ ergs/s. This rate is comparable to that dissipated near the earth during moderate strength substorms, $\langle U_A \rangle \cong 3 \times 10^{18}$ ergs/s (Akasofu, 1977). The near equality of these two numbers may reflect the fact that equal amounts of energy flux are dissipated in the near-earth and distant-tail pairs of slow-mode shocks. The near-earth shocks then funnel their energy into the ring current and auroral ionosphere through particle precipitation and current-driven Joule heating.

The plasmoids released to the solar wind through the far tail represent the last major form of dissipation during substorms. Modifying the estimate made by Scholer *et al.* (1984b) to be consistent with our present estimate for the cross-tail width of the merging region, $w \cong 7$ R_E (they chose $w = 50$ R_E), we find an average energy dissipated in the form of plasmoids, $E_p \cong 7 \times 10^{20}$ ergs. Comparison of this energy with that released during an entire substorm, either through the pair of far-tail slow shocks or to the near-Earth region, shows that plasmoids only represent a minor fraction of the total substorm energy budget. Assuming the average substorm lasts about $\Delta T \cong 1.5$ hours, yields $E_s = \langle U_s \rangle \Delta T = 2.7 \times 10^{22}$ ergs and $E_A = \langle U_A \rangle \Delta T = 1.6 \times 10^{22}$ ergs. We therefore conclude that slow-mode shocks in the geomagnetic tail account for a major part, if not a dominant part, of the energy budget of magnetospheric substorms.

6) Summary and Discussion

Although slow-mode shocks may form in several parts of the terrestrial magnetosphere, they have only

been identified as forming a relatively narrow section of the high-latitude boundary of the plasma sheet. Whereas two views of the geomagnetic tail during "quiet" conditions are shown in Fig. 6, a schematic version showing the central portion of the tail just after plasmoid release during the recovery phase of a substorm, is shown in Fig. 13. Note that for both conditions, the four shock surfaces which fan out from the neutral line may only extend across a small section of the lobe-plasma sheet boundary containing the neutral line. The rest of the surface would then be a tangential discontinuity.

The presence of these shocks affect the properties of a very much larger volume of surrounding plasma. These effects were summarized schematically in Fig. 7. They are seen to be closely analogous to phenomena observed in the near vicinity of the Earth's bow shock. Specifically, both lobes of the geomagnetic tail are analogous to the solar wind, the lobe-plasma sheet boundary layers are analogous to the foreshock of the Earth's bow shock, and the plasma-sheet is analogous to the magnetosheath.

The plasma in the plasma sheet is most directly affected by the slow shocks in the geomagnetic tail since it consists of shock-processed lobe plasma. For the purposes of this review, we adopt as the defining feature of the plasma sheet that the internal energy density of its plasma particles exceeds that in the magnetic field. Although this definition differs, at times, from that adopted by some researchers in the field, it appears to better organize the phenomenology reviewed here. Whistler waves are often seen in this region (Scarf *et al.*, 1984b). In analogy with the earth's bow shock (Tokar *et al.*, 1984), these waves may be generated by electron beams in the shock, and then convected downstream.

A boundary layer upstream of these shocks represents a well-developed slow foreshock. It supports many phenomena observed in the terrestrial bow-wave foreshock (see, e.g., Thomsen, 1985; Klimas, 1985 and references therein). Energetic and suprathermal electrons mark its leading edge followed by streams of suprathermal ions just behind. These ions are predicted to escape in copious numbers to the upstream region in theoretical analyses of slow shocks (Winske *et al.*, 1985; Edmiston and Kennel, 1986; Winske, 1987). Motion of the lobe magnetic fields toward the central plane of the magnetotail enforces a dispersion whereby the fastest particles preferentially populate the outermost (lobeward edge) reaches of the foreshock, and the slower particles add to the total particle population in the inner reaches of the foreshock. This separation results from the fact that suprathermal particles escaping through the entire length of the shock surface, from the shocked downstream medium to the unshocked upstream medium, begin to populate a field line only when it reconnects in a small volume surrounding the neutral line. These limiting field lines

form the separatrix surfaces. Continuing inward convection of lobe field lines then enforces a separation, whereby only those particles having speeds faster than spatially variable limiting values, can reach any given location within the foreshock before the field line convects past. The situation near the geomagnetic tail slow shocks is closely analogous to that occurring upstream of the Earth's bow shock. Small differences are observed and are expected, because the changes in magnetic field magnitude at the bow shock and tail shocks have opposite signs, and because the near earth slow foreshocks close in the ionosphere, whereas the bow-shock and deep-tail slow foreshocks are open to interplanetary space.

The foregoing spatial structure of energetic and suprathermal particles is associated with wave turbulence very similar to that observed in the Earth's foreshock. Broadband electrostatic noise, electron plasma oscillations, and magnetosonic fast-mode waves are observed in the slow-mode foreshocks. Whereas the plasma oscillations are driven by an electron heat flux (Scarf *et al.*, 1984), the fast-mode waves are driven by the streaming ion population (Tsurutani and Smith, 1984; Tsurutani *et al.*, 1985). These fast-mode waves have k vectors pointing away from the shock within a cone angle of about 20°. The origin of the broadband electrostatic noise has not yet been identified.

Since the wave turbulence measured upstream from the slow shocks in the geomagnetic tail is very similar to that measured upstream of the bow shock, it is reasonable to inquire whether slow shocks accelerate particles as efficiently as do fast shocks. A search for signatures of such acceleration upstream from the distant-tail slow shocks have so far proved disappointing (Sanderson and Wenzel, 1985). A possible reason for this lack of acceleration may be that, in contrast to the case upstream of fast shocks, the self-generated magnetosonic waves upstream of slow shocks escape outward since they can travel faster than the shock (Isenberg, 1986). They therefore do not satisfy the requirements necessary for a first-order Fermi process.

Not much is known observationally about the internal structure of slow shocks because of a lack of analyses of adequate data. One feature found commonly within the earth's bow shock (Feldman *et al.*, 1982) that occurs within the slow shocks in the geomagnetic tail (Feldman *et al.*, 1984) are downstream propagating electron beams. These beams are thought to result from acceleration across the shock by an electrostatic potential difference averaging several hundred volts (e.g., Feldman, 1985b, and references therein; Schwartz *et al.*, 1987).

Other features of slow-shock structure are known only through the detailed analysis of one event, that

observed in the near tail on 24 April 1979 (Feldman *et al.*, 1987). This shock was moderately strong. It had a slow-mode Mach number between 3.2 and 4.0, slightly less than the average of those observed in the distant tail, $\langle M_{sm} \rangle = 4.7$, and an Alfvén Mach number between 0.10 and 0.67, in range of the average of the distant-tail shocks, $\langle M_A \rangle = 0.19$. Two points of special note is a measurement of its thickness and the observation of a trailing, large-amplitude ion-cyclotron wave. This thickness turned out to be very close to the upstream ion inertial length, c/ω_{pi_u}, and to the wavelength of the trailing ion-cyclotron wave. The fact that this wavelength was just that needed to stand in the instreaming flow suggests that the shock wave-front steepness was limited by dispersion rather than anomalous resistivity. This result is consistent with the fact that the measured intensity of electrostatic turbulence in the deep-tail shocks was not sufficiently high to arrest further steepening (Scarf *et al.*, 1984b). However, similar trains of trailing ion-cyclotron waves have not yet been identified in the distant geomagnetic tail.

We note, though, that the distant tail plasma sheet appears much thinner than does the near-Earth plasma sheet. The two shocks bounding the distant plasma sheet may therefore interact through their common downstream plasmas. Perhaps such an interaction has modified the structure of trailing ion-cyclotron waves in the distant plasma sheet so that their structure differs from that single wave evident in the example of a near-Earth slow-shock crossing shown in Fig. 11. The fact that the Y-component of the magnetic field downstream, of most of the deep-tail shocks studied to date, has the same orientation, as that shown in Figs. 3 and 4, supports this suggestion. A single 180° turn of $\overline{B}$ through positive B_y (a dawn to dusk orientation, as evident in Fig. 3) has just the orientation expected of a large-amplitude ion-cyclotron wave trailing both north- and south-bounding shocks. This structure, if a wave, would have normals directed upstream at both slow-shock boundaries. However, it is also possible that the variation in the azimuth of $\overline{B}$, evident between 1840 UT and 1910 UT in Fig. 4, is the conventional magnetic signature of a trailing ion-cyclotron wave. A note of caution is in order here. As just mentioned, trailing ion-cyclotron waves have not yet been definitively identified in the distant geomagnetic tail. Such identification requires ion and electron fluid parameters in addition to $\overline{B}$. Since ion data were not available on ISEE 3, resolution of this issue requires new measurements in the distant geomagnetic tail.

We now return to the role slow shocks play in geomagnetic substorms. They have been found to bound the high-latitude plasma sheet in the distant tail during all phases of geomagnetic activity and so are a semipermanent structural entity of the distant tail (Feldman *et al.*, 1984b). An estimate of the

average power they dissipate in the form of converting a Poynting flux into a bulk kinetic energy flux, a convected enthalpy, and a heat flux, shows that they play an important, if not dominant role in the dynamics of the distant geomagnetic tail. Comparison with the power dissipated near the earth during moderate strength substorms (Akasofu, 1977), shows the two are comparable. Although only one slow shock has been identified on the earthward side of the neutral line to date, this close comparison between distant- and near-Earth tail power budgets suggests that most of the power dissipated near the Earth in the form of ring current build up, particle precipitation in the auroral zone, and Joule heating of the auroral ionosphere during substorms, may be supplied by near-Earth slow-mode shocks. We therefore agree with the conclusion of Eastman and coworkers (Eastman *et al.*, 1984, 1985; Eastman and Frank, 1984; Frank, 1985) that slow-mode shocks and their upstream foreshocks, which comprise the high latitude plasma-sheet boundary layer, play an important role in the dynamics of geomagnetic substorms. However, in contrast to their paradigm of magnetospheric activity that pictures substorm onset as caused by the earthward motion of sporadically formed neutral lines in the distant tail (so called "fireballs," Frank *et al.*, 1976; Frank, 1985), we find the evidence supporting the alternative paradigm of geomagnetic activity sketched in Fig. 12 (e.g., Russell and McPherron, 1973; Hones, 1979; Nishida, 1984, and references therein) overwhelming. In this latter view, a southward-turning magnetic field in the solar wind initiates enhanced reconnection on the front side of the magnetopause. Subsequent convection of magnetic field lines, from the front side of the magnetosphere over the polar caps to the tail, leads to the transfer of energy across the magnetopause to magnetic energy where it is stored temporarily in the lobes of the geomagnetic tail. Substorm initiation is then marked by formation of a new neutral line in the near-earth tail leading to plasmoid ejection in addition to all the phenomenology that both paradigms have in common.

The morphology of structural changes which occur during geomagnetic substorms is closely similar to that used to describe two-ribbon solar flares (Sturrock, 1968; Kopp and Pneuman, 1976; Cargill and Priest, 1983; Forbes, 1986; Forbes and Malherbe, 1986). The similarities are evident by contrasting a figure from Forbes and Malherbe (1986), shown here as Fig. 14, with Figs. 6 and 7 of this review. Although the phenomenology known to occur in the geomagnetic tail is much more detailed and complete because of the wealth of measurements made using in situ satellite probes, corresponding structures are easily identified. For example, the conduction front in Fig. 14 can be associated with the bidirectional (or, at times, nearly isotropic) fluxes of energetic electrons found between the separatrix and the plasma-sheet

boundary in the near tail; the H_α ribbons correspond to the discreet auroras; the upward streaming evaporated chromospheric plasma corresponds to the beams of ionospheric ions propagating tailward and observed to be enhanced near the plasma sheet boundary (Ghielmetti *et al.*, 1978; Sharp *et al.*, 1981; Gorney *et al.*, 1981; Collin *et al.*, 1981; Eastman *et al.*, 1984); and the deflection sheath H_α loop-prominence corresponds to the earthward plasma-sheet jets which are slowed by, and diverted around, the stationary plasma sheet. The only element included in the two-ribbon solar-flare configuration not observed in the near magnetotail is the fast-mode shock at the base of the narrow, downward jet which feeds the H_α loop prominence. No such shock was necessary in the single magnetotail event studied to date because the speed of the jet in this event was less than the downstream Alfvén speed. Perhaps such a shock may appear during other, more energetic substorms that support higher Mach number slow-mode shocks in the near-earth geomagnetic tail.

Acknowledgments. We wish to thank D. Winske for a careful reading of the manuscript. This research was conducted under the auspices of the U.S. Department of Energy.

References

Akasofu, S.-I., "Physics of Magnetospheric Substorms," p. 274, D. Reidel Publ. Co., Dordrecht-Holland, 1977.

Andrews, M. K., P. W. Daly, and E. Keppler, Ion jetting at the plasma sheet boundary: simultaneous observations of incident and reflected particles, *Geophys. Res. Lett.*, **8**, 987, 1981.

Baker, D. N., and E. C. Stone, Energetic electron anisotropies in the magnetotail: identification of open and closed field lines, *Geophys. Res. Lett.*, **3**,557, 1976.

Baker, D. N., and E. C. Stone, Observations of energetic electrons ($E \lesssim 200$ keV) in the Earth's magnetotail: plasma sheet and fireball observations, *J. Geophys. Res.*, **82**, 1532, 1977.

Bieber, J. W., Streaming energetic electrons in reconnection events, in "Magnetic Reconnection in Space and Laboratory Plasmas," *Geophys. Monogr. Ser.*, Vol. 30, E. W. Hones, Jr., ed., p. 185, AGU, Washington, DC, 1984.

Bieber, J. W., and E. C. Stone, Streaming energetic electrons in the Earth's magnetotail: evidence for substorm-associated magnetic reconnection, *Geophys. Res. Lett.*, **7**, 945, 1980.

Bieber, J. W., and E. C. Stone, Plasma behavior during energetic electron streaming events: further evidence for substorm-associated magnetic reconnection, *Geophys. Res. Lett.*, **9**, 664, 1982.

Cargill, P. J., and E. R. Priest, Slow-shock heating and the Kopp-Pneuman model for "post"-flare loops, *Solar Phys.*, **76**, 357, 1982.

Cattell, C. A., M. Kim, R. P. Lin, and F. S. Mozer, Observations of large electric fields near the plasma sheet boundary by ISEE-1, *Geophys. Res. Lett.*, **9**, 539, 1982.

Colburn, D. S., and C. P. Sonett, Discontinuities in the solar wind, *Space Sci. Rev.*, **5**, 439, 1966.

Collin, H. L., R. D. Sharp, E. G. Shelley, and R. D. Johnson, Some general characteristics of upflowing ion beams over the auroral zone and their relationship to auroral electrons, *J. Geophys. Res.*, **86**, 6820, 1981.

Coroniti, F. V., Laminer wave-train structure of collisionless magnetic slow shocks, *Nucl. Fusion*, **11**, 261, 1971.

Cowley, S. W. H., R. J. Hynds, I. G. Richardson, P. W. Daly, T. R. Sanderson, K.-P. Wenzel, J. A. Slavin, and B. T. Tsurutani, Energetic ion regimes in the deep geomagnetic tail: ISEE-3, *Geophys. Res. Lett.*, **11**, 275, 1984.

Dungey, J. W., Interplanetary magnetic field and the auroral zone, *Phys. Rev. Lett.*, **6**, 47, 1961.

Decoster, R. J., and L. A. Frank, Observations pertaining to the dynamics of the plasma sheet, *J. Geophys. Res.*, 84, 5099, 1979.

Eastman, T. E., and L. A. Frank, Boundary layers of the Earth's outer magnetosphere, in "Magnetic Reconnection in Space and Laboratory Plasmas," *Geophys. Monogr. Ser.*, Vol. 30, p. 249, AGU, Washington, DC, 1984.

Eastman, T. E., L. A. Frank, W. K. Peterson, and W. Lennartsson, The plasma sheet boundary layer, *J. Geophys. Res.*, **89**, 1553, 1984.

Eastman, T. E., L. A. Frank, and C. Y. Huang, The boundary layers as the primary transport regions of the Earth's magnetotail, *J. Geophys. Res.*, **90**, 9541, 1985.

Edmiston, J. P., and C. F. Fennel, A parametric study of slow shock Rankine-Hugoniot solutions and critical Mach numbers, *J. Geophys. Res.*, **91**, 1361, 1986.

Feldman, W. C., Electron velocity distributions near collisionless shocks, in "Collisionless Shocks in the Heliosphere: Reviews of Current Research," B. T. Tsurutani and R. G. Stone, eds., *Geophys. Monogr. Ser.*, Vol. 35, p. 195, AGU, Washington, DC, 1985b.

Feldman, W. C., S. J. Schwartz, S. J. Bame, D. N. Baker, J. Birn, J. T. Gosling, E. W. Hones, Jr., D. J. McComas, J. A. Slavin, E. J. Smith, and R. D. Zwickl, Evidence for slow-mode shocks in the deep geomagnetic tail, *Geophys. Res. Lett.*, **11**, 599, 1984a.

Feldman, W. C., D. N. Baker, S. J. Bame, J. Birn, E. W. Hones, Jr., S. J. Schwartz, and R. L. Tokar, Power dissipation at slow-mode shocks in the distant geomagnetic tail, *Geophys. Res. Lett.*, **11**, 1058, 1984b.

Feldman, W. C., D. N. Baker, S. J. Bame, J. Birn, J. T. Gosling, E. W. Hones, Jr., and S. J. Schwartz, Slow-mode shocks: a semipermanent feature of the distant geomagnetic tail, *J. Geophys. Res.*, **90**, 233, 1985a.

Feldman, W. C., R. L. Tokar, J. Birn, E. W. Hones, Jr., S. J. Bame, and C. T. Russell, Structure of a slow-mode shock observed in the plasma sheet boundary layer, *J. Geophys. Res.*, **92**, 83, 1987.

Fennell, J. F., Access of solar protons to the Earth's polar caps, *J. Geophys. Res.*, **78**, 1036, 1973.

Forbes, T. G., Fast-shock formation in line-tied magnetic reconnection models of solar flares, *Astrophys. J.*, **305**, 553, 1986.

Forbes, T. G., E. W. Hones, Jr., S. J. Bame, J. R. Asbridge, G. Paschmann, N. Sckopke, and C. T. Russell, Evidence for the Tailward retreat of a magnetic neutral line in the magnetotail during substorm recovery, *Geophys. Res. Lett.*, **8**, 261, 1981.

Forbes, T. G., and J. M. Malherbe, A shock condensation mechanism for loop prominences, *Astrophys. J.*, **302**, L67, 1986.

Frank, L. A., Plasmas in the Earth's magnetotail, *Space Sci. Rev.*, **42**, 211, 1985.

Frank, L. A., K. L. Ackerson, and R. P. Lepping, On hot tenuous plasmas, fireballs, and boundary layer in the Earth's magnetotail, *J. Geophys. Res.*, **81**, 5859, 1976.

Frank, L. A., R. L. McPherron, R. J. Decoster, B. G. Burek, K. L. Ackerson, and C. T. Russell, *J. Geophys. Res.*, **86**, 687, 1981.

Ghielmetti, A. G., R. G. Johnson, R. D. Sharp, and E. G. Shelley, The latitudinal, diurnal, and altitudinal distribution of upward flowing energetic ions of ionospheric origin, *Geophys. Res. Lett.*, **5**, 59, 1978.

Gorney, D. J., A. Clarke, D. R. Croley, J. F. Fennell, M. Luhmann, and P. F. Mizera, The distribution of ion beams and conics below 8000 km, *J. Geophys. Res.*, **86**, 83, 1981.

Gosling, J. T., M. F. Thomsen, S. J. Bame, and C. T. Russell, Accelerated plasma flows at the near-tail magnetopause, *J. Geophys. Res.*, **91**, 3029, 1986.

Gurnett, D. A., L. A. Frank, and R. P. Lepping, Plasma waves in the distant magnetotail, *J. Geophys. Res.*, **81**, 6059, 1976.

Hada, T., and C. F. Kennel, Nonlinear evolution of slow waves in the solar wind, *J. Geophys. Res.*, **90**, 531, 1985.

Hones, E. W., Jr., Plasma flow in the magnetotail and its implications for substorm theories, in "Dynamics of the Magnetosphere," S.-I. Akasofu, ed., D. Reidel Publ. Co., p. 545, 1979.

Ipavich, F. M., A. B. Galvin, G. Gloeckler, D. Hovestadt, B. Klecker, and M. Scholer, Energetic (> 100 keV)O^+ ions in the plasma sheet, *Geophys. Res. Lett.*, **11**, 504, 1984.

Isenberg, P. A., On a difficulty with accelerating particles at slow-mode shocks, *J. Geophys. Res.*, **91**, 1699, 1986.

Klimas, A. J., The electron foreshock, in "Collisionless Shocks in the Heliosphere: Reviews of Current Research," B. T. Tsurutani and R. G. Stone, eds., *Geophysical Monograph Ser.*, Vol. 35, American Geophysical Union, Washington, DC, p. 237, 1985.

Kopp, R. A., and G. W. Pneuman, Magnetic reconnection in the corona and the loop prominence phenomenon, *Solar Phys.*, **50**, 85, 1976.

Levy, R. H., H. E. Petchek, and G. L. Siscoe, Aerodynamic aspects of magnetospheric flow, *AIAA Journal*, **2**, 2065. 1964.

Lui, A. T. Y., E. W. Hones, Jr., F. Yasuhara, S.-I. Akasofu, and S. J. Bame, Magnetotail plasma flow during plasma sheet expansions: Vela 5 and 6 and IMP 6 observations, *J. Geophys. Res.*, **82**, 1235, 1977.

Lui, A. T. Y., T. E. Eastman, D. J. Williams, and L. A. Frank, Observations of ion streaming during substorms, *J. Geo Res.*, **88**, 7753, 1983.

Möbius, E., F. M. , M. Scholer, G. Gloeckler, D. Hovestadt, and B. Klecker, Observations of a nonthermal ion layer at the plasma sheet boundary during substorm recovery, *J. Geophys. Res.*, **85** 5143, 1980.

Nishida, A., Reconnection in Earth's magnetotail: An overview, in "Magnetotail Reconnection in Space and Laboratory Plasmas," *Geophys. Monogr. Ser.*, Vol. 30, E. W. Hones, Jr., ed., p. 159, AGU, Washington, DC, 1984.

Orsini, S., M. Candidi, V. Formisano, H. Balsiger, A. Ghielmetti, and K. W. Ogilvie, The structure of the plasma sheet-lobe boundary in the Earth's magnetotail, *J. Geophys. Res.*, **89**, 1573, 1984.

Parks, G. K., M. McCarthy, R. J. Fitzenreiter, J. Etcheto, K. A. Anderson, R. R. Anderson, T. E. Eastman, L. A. Frank, D. A. Gurnett, C. Huang, R. P. Lin, A. T. Y. Lui, K. W. Ogilvie, A. Pedersen, H. Reme, and D. J. Williams, Particle and field characteristics of the high-latitude plasma sheet boundary layer, *J. Geophys. Res.*, **89**, 8885, 1984.

Pedersen, A., C. A. Cattell, C.-G. Fälthammer, K. Knott, P.-A. Lindquist, R. H. Manka, and F. S. Mozer, Electric fields in the plasma sheet and plasma sheet boundary layer, *J. Geophys. Res.*, **90**, 1231, 1985.

Petchek, H. E., Magnetic field annihilation, in "AAS-NASA Symposium on Solar Flares," NASA SP-50, Washington, DC, p. 334, 1964.

Pudovkin, M. I., and V. S. Semenov, Magnetic field reconnection theory and the solar wind-magnetosphere interaction: a review, *Space Sci. Rev.*, **41**, 1, 1985.

Reiff, P. H., R. W. Spiro, and T. W. Hill, Dependence of polar cap potential drop on interplanetary parameters, *J. Geophys. Res.*, **86**, 7639, 1981.

Richardson, I. G., and S. W. H. Cowley, Plasmoid-associated energetic ion bursts in the deep geomagnetic

tail: properties of the boundary layer, *J. Geophys. Res.*, **90**, 12133, 1985.

Russell, C. T., and R. L. McPherron, The magnetotail and substorms, *Space Sci. Rev.*, **15**, 205, 1973.

Scarf, F. L., L. A. Frank, K. L. Ackerson, and R. P. Lepping, Plasma wave turbulence at distant crossings of the plasma sheet boundaries and the neutral sheet, *Geophys. Res. Lett.*, **1**, 189, 1974.

Scarf, F. L., F. V. Coroniti, C. F. Kennel, R. W. Fredricks, D. A. Gurnett, and E. J. Smith, ISEE-3 wave measurements in the distant geomagnetic tail and boundary layer, *Geophys. Res. Lett.*, **11**, 335, 1984a.

Scarf, F. L., F. V. Coroniti, C. F. Kennel, E. J. Smith, J. A. Slavin, B. T. Tsurutani, S. J. Bame, and W. C. Feldman, Plasma wave spectra near slow mode shocks in the distant magnetotail, *Geophys. Res. Lett.*, **11**, 1050, 1984b.

Scholer, M., G. Gloeckler, B. Klecker, F. M. Ipavich, D. Hovestadt, and E. J. Smith, Fast moving plasma structures in the distant magnetotail, *J. Geophys. Res.*, **89**, 6717, 1984.

Scholer, M., G. Gloeckler, D. Hovestadt, B. Klecker, and F. M. Ipavich, Characteristics of plasmoidlike structures in the distant magnetotail, *J. Geophys. Res.*, **89**, 8872, 1984b.

Schwartz, S. J., M. F. Thomsen, W. C. Feldman, and F. T. Douglas, Electron dynamics and potential jump across slow mode shocks, *J. Geophys. Res.*, **92**, 3165, 1987.

Sharp, R. D., D. L. Carr, W. K. Peterson, and E. G. Shelley, Ion streams in the magnetotail, *J. Geophys. Res.*, **86**, 4639, 1981.

Smith, E. J., J. A. Slavin, B. T. Tsurutani, W. C. Feldman, and S. J. Bame, Slow mode shocks in the Earth's magnetotail: ISEE-3, *Geophys. Res. Lett.*, **11**, 1054, 1984.

Spjeldvik, W. N., and T. A. Fritz, Energetic ion and electron observations of the geomagnetic plasma sheet boundary layer: three-dimensional results from ISEE 1, *J. Geophys. Res.*, **86**, 2480, 1981.

Sturrock, P. A., A model of solar flares, in "Structure and Development of Active Regions," K. O. Kiepenheuer, ed., IAU Symp. 35, p. 471, 1968.

Swift, D. W., On the structure of the magnetic slow switch-off shock, *J. Geophys. Res.*, 88, 5685, 1983.

Thomsen, M. F., Upstream suprathermal ions, in "Collisionless Shocks in the Heliosphere: Reviews of Current Research," B. T. Tsurutani and R. G. Stone, eds., *Geophysical Monograph Ser*, Vol. 35, American Geophysical Union, Washington, DC, p. 253, 1985.

Tokar, R. L., D. A. Gurnett, and W. C. Feldman, Whistler mode turbulence generated by electron beams in Earth's bow shock, *J. Geophys. Res.*, **89**, 105, 1984.

Tsurutani, B. T., and E. J. Smith, Magnetosonic waves adjacent to the plasma sheet in the distant magnetotail: ISEE-3, *Geophys. Res. Lett.*, **11**, 331, 1984.

Tsurutani, B. T., I. G. Richardson, R. M. Thorne, W. Butler, E. J. Smith, S. W. H. Cowley, S. P. Gary, S.-I. Akasofu, and R. D. Zwickl, Observations of the right-hand resonant ion beam instability in the distant plasma sheet boundary layer, *J. Geophys. Res.*, **90**, 12159, 1985.

West, H. I., Jr., and A. L. Vampola, Simultaneous observations of solar flare electron spectra in interplanetary space and within the Earth's magnetosphere, *Phys. Rev. Lett.*, **26**, 458, 1971.

Williams, D. J., Energetic ion beams at the edge of the plasma sheet: ISEE 1 observations plus a simple explanatory model, *J. Geophys. Res.*, **86**, 5507, 1981.

Winske, D., Numerical modeling of slow shocks, in "Proceedings of Solar Wind Six," Estes Park, Colorado, 1987.

Winske, D., E. K. Stover, and S. P. Gary, The structure and evolution of slow mode shocks, *Geophys. Res. Lett.*, **12**, 295, 1985.

Zwickl, R. D., D. N. Baker, S. J. Bame,W. C. Feldman, J. T. Gosling, E. W. Hones, Jr., D. J. McComas, B. T. Tsurutani, and J. A. Slavin, Evolution of the Earth's distant magnetotail: ISEE 3 electron plasma results, *J. Geophys. Res.*, **89**, 11007, 1984.

Figure Captions

Figure 1 A schematic representation of reconnection at the subsolar magnetopause identifying the various MHD structures expected. The magnetopause consists of a leading rotational discontinuity and a trailing slow-mode expansion wave. This expansion wave has been identified observationally as the solar wind-magnetosphere boundary layer. This figure is reproduced from Levy *et al.* (1964).

Figure 2 Schematic view of the reconnection topology in the geomagnetic tail. Field lines are shown by single arrows while double arrows denote bulk velocities. The dashed lines represent the separatrices across which the magnetic topology changes. Plasma flows in toward the X-axis from both lobes and is turned tailward or earthward on crossing the slow shocks (heavy solid lines) into the plasma sheet. Details, showing a coordinate system relevant to that part of the slow-shock boundary encircled at the lower right of the view on top, are given below. This figure is reproduced from Feldman *et al.* (1984a).

Figure 3 A plot of the plasma electron density, N, tailward component of the bulk speed, V_x, temperature, T_e, and heat flux, Q_e, along with the polar coordinates (in the GSE frame) of the magnetic field vector, (B, θ, ϕ) for a complete crossing of the plasma sheet (approximately indicated by the hatched region) from the north lobe ($\phi \simeq 0°$) to the south lobe ($\phi \simeq 180°$) on 23 March 1983. This figure is reproduced from Feldman *et al.* (1984a).

Figure 4 A plot of the plasma electron density, N, bulk plasma speed, V, electron temperature, T_e, and heat flux, Q_e, along with the polar coordinates (in the GSE frame) of the magnetic vector (B, θ, ϕ), during a 3-hour period on 2 February 1983. The hatched region shows when ISEE 3 encountered the neutral sheet bounded by slow-mode shocks at about 1828 UT and 1922 UT, respectively. This figure is reproduced from Feldman *et al.* (1985b).

Figure 5 Cuts through three electron velocity distributions parallel to $\overline{B}$, measured across the slow-mode shock encountered at 1922 UT on 2 February 1983. The solid curve overlaying the lobe distribution at 1922:45 UT gives the Gaussian which fits best the inner six energy points. The hatched region between the measured distribution and the Gaussian function accentuates the heat flux flowing in the lobe away from the shock. Positive speeds are along $\overline{B}$ but in general direction toward the Earth. Hence, the lobe heat flux is oriented tailward (negative $V_{\|}$). This figure is reproduced from Feldman *et al.* (1985b).

Figure 6 Two schematic views of the geomagnetic tail showing a noon-midnight meridional cut (above) and a dawn-dusk cut (below) through the tail somewhat downstream of the neutral line (shown by the

A-A vector in the meridional cut). The boundary layer is accentuated by hatch marks, the plasma sheet by cross-hatch marks, and the whole-tail boundary layer by the stipling. The thick solid lines mark the slow-mode shock and the dashed lines mark the separatrices.

Figure 7 A schematic overview of the various particle populations and their self-generated wave fields present in the neighborhood of the high-latitude boundaries of the plasma sheet in the geomagnetic tail. The linear arrays of minus signs denote the leading edges of the electron foreshocks and the linear arrays of plus signs denote the leading edges of the ion foreshocks.

Figure 8 Details of the magnetic intensity, B, and the number density, X-component of the proton bulk flow velocity, electron temperature, and proton temperature during the recovery phase of the substorm on 24 April 1979. The numbers from one through four at the top give the times when electron spectra shown in Figure 10 were measured. The tops and bottoms of the vertical lines in both temperature plots give the maximum and minimum diagonal elements of respective electron and proton temperature tensors. The cross-hatched regions labeled u and $d1$ in the electron temperature plot identify those intervals for evaluating upstream and downstream parameters using a one-fluid Rankine-Hugoniot analysis. This figure is reproduced from Feldman *et al.* (1985a).

Figure 9 Thirty-second averages of the proton heat flux calculated at 15-second intervals. The sign of the heat flux is positive or negative depending whether the X component points earthward or tailward, respectively. The error bars give the standard deviations of the means estimated from the variance of the distribution of three-second samples within each 30-second interval. This figure is reproduced from Feldman *et al.* (1985a).

Figure 10 Parallel and perpendicular (to $\overline{B}$) cuts through electron velocity distributions measured at the times indicated by the respective numbers at the top of Figure 8. The smooth curves give the best Gaussian fits to each of the perpendicular cuts, and the data points with connecting lines give the parallel cuts. This figure is reproduced from Feldman *et al.* (1985a).

Figure 11 Thirty-second averages of the X and Y components of the proton and electron bulk velocities during the recovery phase of the 24 April 1979 substorm. The dots give the electron means calculated every 15 seconds, the vertical lines give the standard deviations of these means estimated from the variance of the distribution of three-second samples within each 30-second interval, and the solid lines give the proton means. The Y components of $\overline{B}$ and $\overline{V}_p$ weighted by $[4\pi N m_p]^{\frac{1}{2}}$ are overlaid in the bottom panel. Their

relative zeros have been shifted so that they are equal at 1143 UT. The hatched region shows the region of strong electron heating, and the cross-hatched regions identify the interval of time when $-B_y$ and $V_y[4\pi N m_p]^{\frac{1}{2}}$ follow each other very closely. This figure is reproduced from Feldman *et al.* (1985a).

Figure 12 Plasma sheet configuration changes during a substorm. Magnetic field lines 1, 2, 3, 4 are in the plasma sheet (fine hatching), field line 5 bounds the presubstorm plasma sheet, and field lines 6 and 7 are initially in the tail lobe. N marks the location of a distant neutral line that terminates the closed pre-substorm plasma sheet. N' marks a neutral line newly formed at substorm onset. Coarse shading represents lobe plasma that has come through the slow-mode shock bounding the plasma sheet and has been accelerated. White arrows indicate directions and approximate relative magnitudes of plasma flows. This figure is reproduced from Hones, 1979.

Figure 13 Schematic drawing of the lobe-plasma sheet boundary configuration of the geomagnetic tail after substorm onset resulting in the formation and tailward ejection of a plasmoid. The view is from the north so that the Earth is toward the upper left and the dawn flank is toward the upper right. The part of the boundary within the two horizontal lines bounding the neutral line is a show-mode shock and that part outside these lines is a tangential discontinuity. This figure is reproduced from Feldman *et al.* (1985a).

Figure 14 Schematic drawing showing the MHD shocks generated by reconnection in a line-tied configuration meant to represent a two-ribbon solar flare. Dashed lines denote magnetic field lines, and dashed-dot lines, the conduction fronts generated by field annihilation at the slow-mode shocks. The correspondence between component parts of this configuration and the phenomenology of geomagnetic substorms summarized in Figure 7, is given in the text. This figure is reproduced from Forbes and Malherbe (1986).

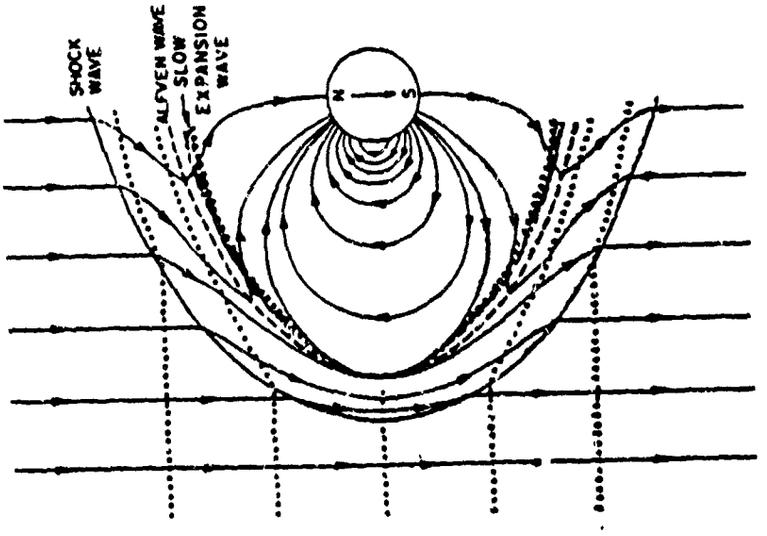

FIG 1

(a)

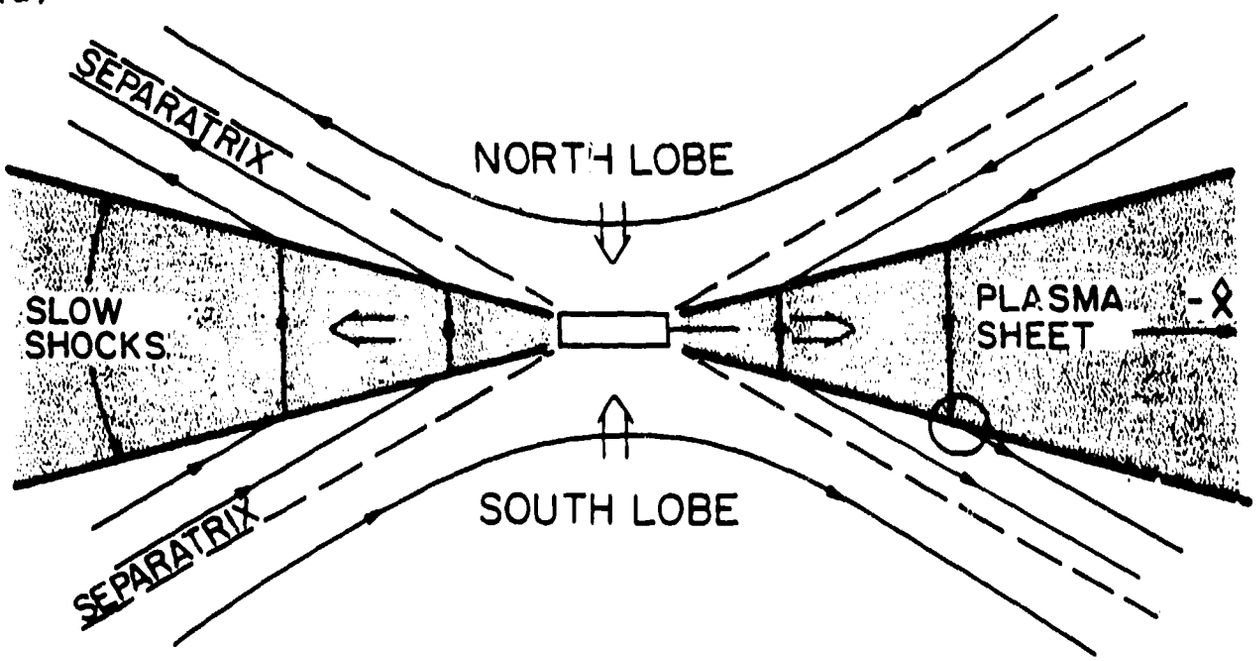
SEPARATRIX
NORTH LOBE
SLOW SHOCKS
PLASMA SHEET
-X
SOUTH LOBE
SEPARATRIX

(b)

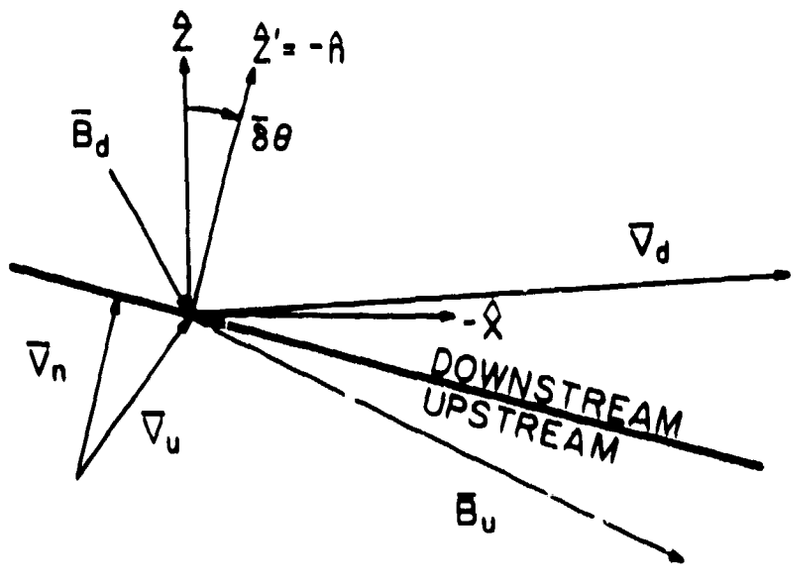
Ẑ
Ẑ' = -A
B̄d
δθ
∇d
-X
∇n
∇u
DOWNSTREAM
UPSTREAM
B̄u

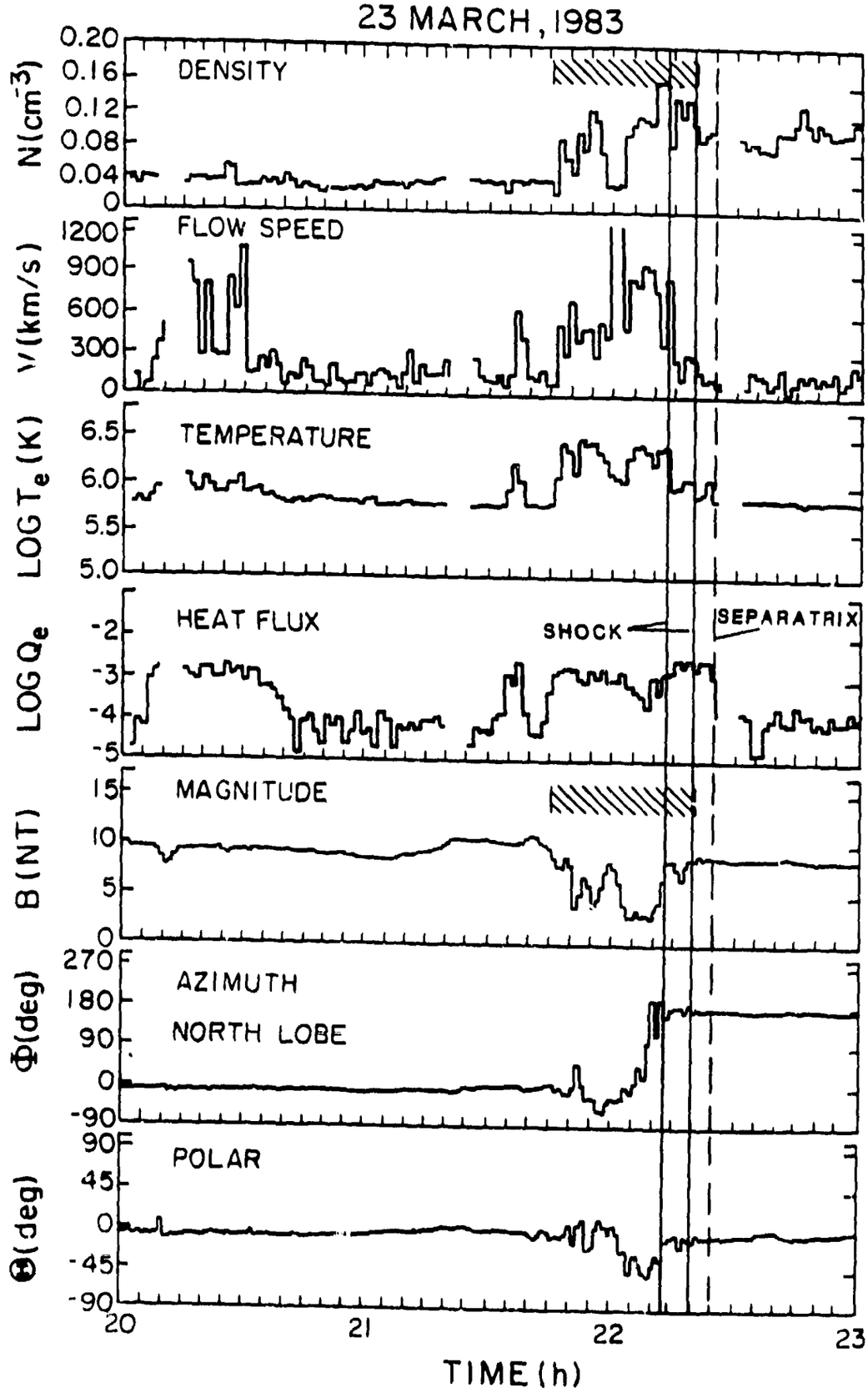
23 MARCH, 1983
DENSITY
N(cm⁻³)
0.20
0.16
0.12
0.08
0.04
0
FLOW SPEED
V(km/s)
1200
900
600
300
0
TEMPERATURE
LOG Te (K)
6.5
6.0
5.5
5.0
HEAT FLUX
LOG Qe
SHOCK
SEPARATRIX
-2
-3
-4
-5
MAGNITUDE
B (NT)
15
10
5
0
AZIMUTH
NORTH LOBE
Φ(deg)
270
180
90
0
-90
POLAR
Θ(deg)
90
45
0
-45
-90
20
21
22
23
TIME (h)

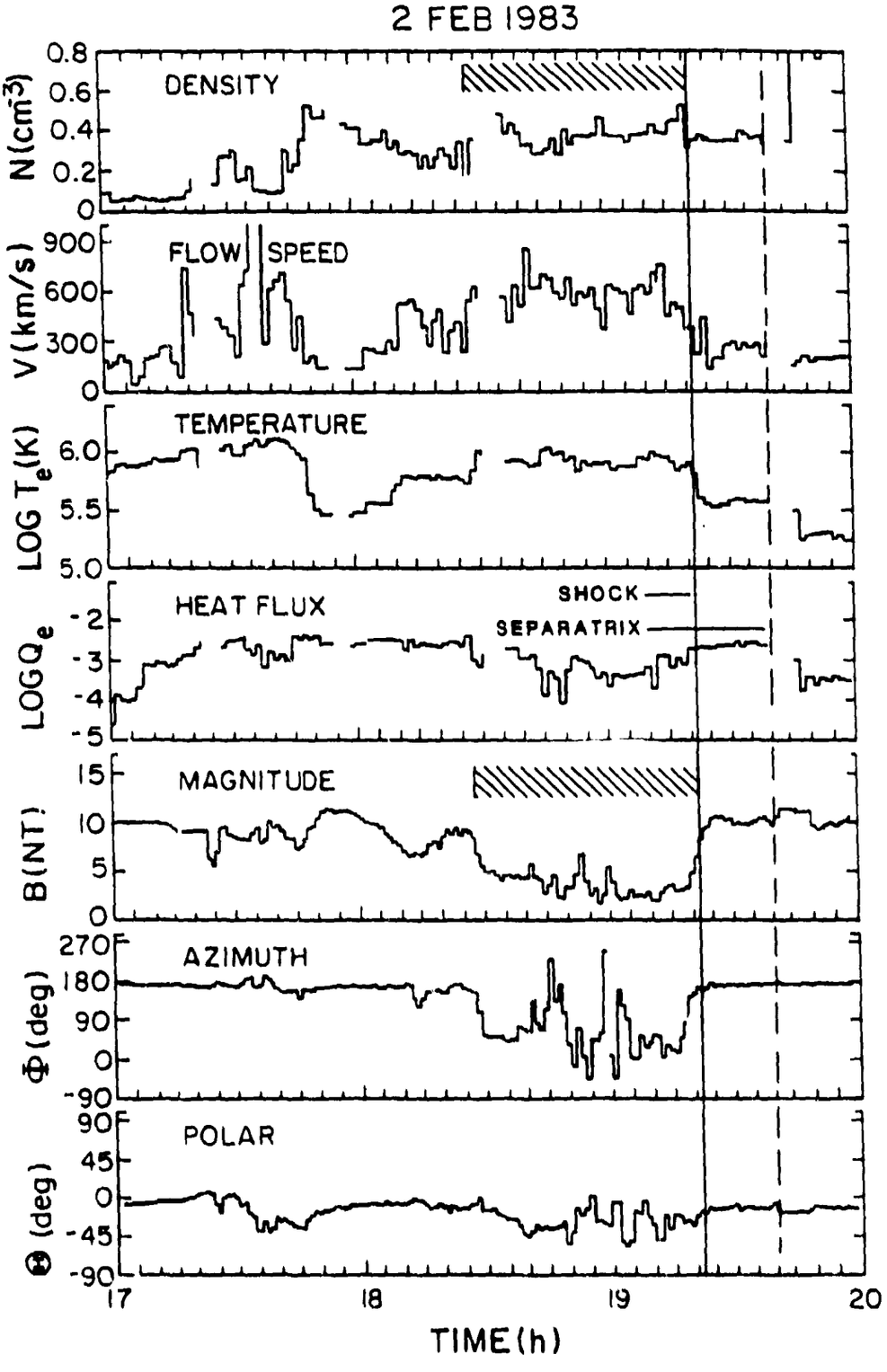
2 FEB 1983
DENSITY
N(cm⁻³)
0.8
0.6
0.4
0.2
0
FLOW SPEED
V(km/s)
900
600
300
0
TEMPERATURE
LOG Te(K)
6.0
5.5
5.0
HEAT FLUX
SHOCK
SEPARATRIX
LOGQe
-2
-3
-4
-5
MAGNITUDE
B(NT)
15
10
5
0
AZIMUTH
Φ(deg)
270
180
90
0
-90
POLAR
Θ (deg)
90
45
0
-45
-90
17
18
19
20
TIME(h)

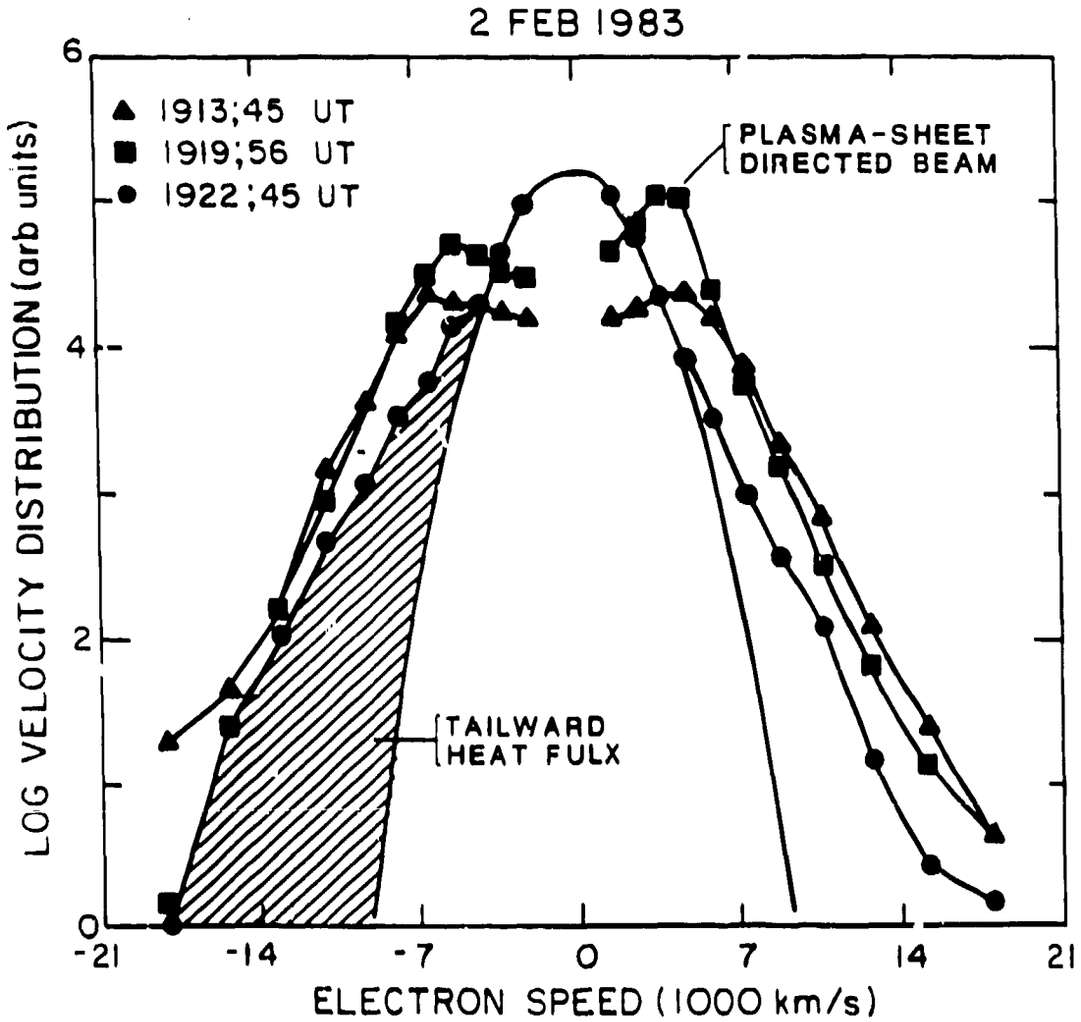
2 FEB 1983
▲ 1913;45 UT
■ 1919;56 UT
● 1922;45 UT
PLASMA-SHEET
DIRECTED BEAM
TAILWARD
HEAT FULX
LOG VELOCITY DISTRIBUTION (arb units)
ELECTRON SPEED (1000 km/s)
6
4
2
0
-21
-14
-7
0
7
14
21

Fig. 5

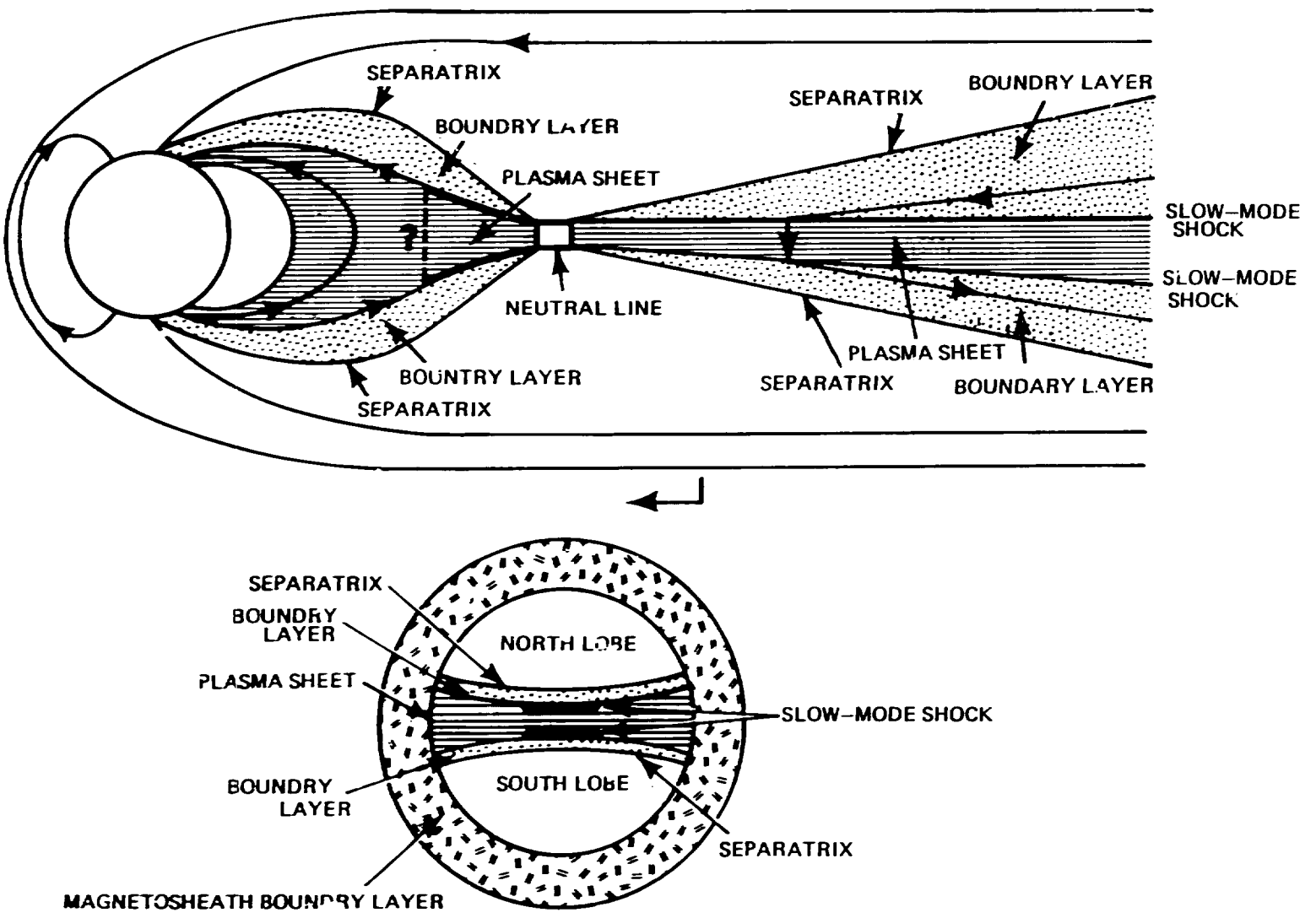
SEPARATRIX
BOUNDRY LAYER
PLASMA SHEET
NEUTRAL LINE
BOUNTRY LAYER
SEPARATRIX
SEPARATRIX
BOUNDRY LAYER
SLOW-MODE SHOCK
SLOW-MODE SHOCK
PLASMA SHEET
SEPARATRIX
BOUNDARY LAYER
SEPARATRIX
BOUNDRY LAYER
PLASMA SHEET
NORTH LOBE
SLOW-MODE SHOCK
SOUTH LOBE
BOUNDRY LAYER
SEPARATRIX
MAGNETOSHEATH BOUNDRY LAYER

FIG 6

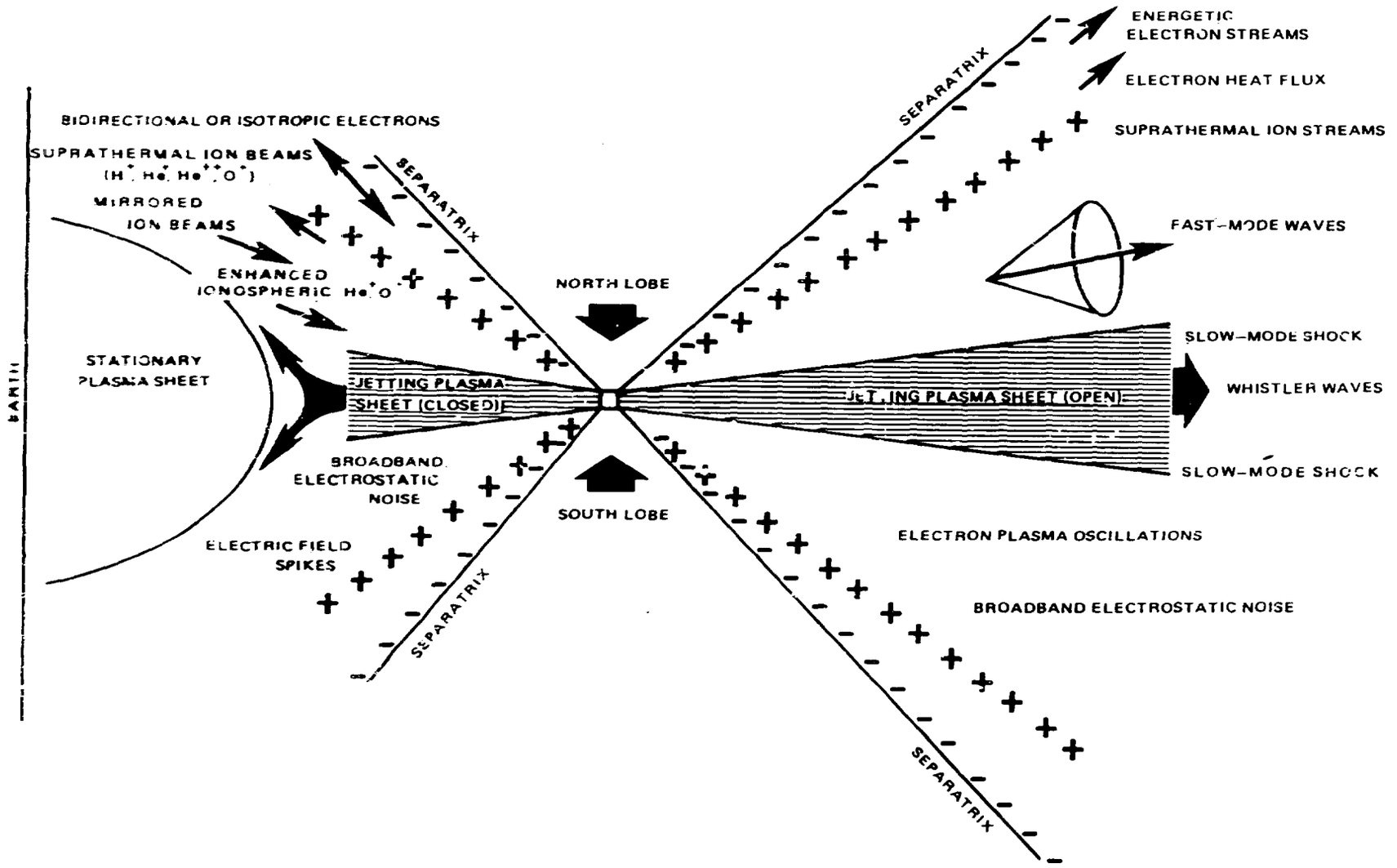
BIDIRECTIONAL OR ISOTROPIC ELECTRONS
SUPRATHERMAL ION BEAMS
MIRRORED ION BEAMS
ENHANCED IONOSPHERIC
STATIONARY PLASMA SHEET
JETTING PLASMA SHEET (CLOSED)
BROADBAND ELECTROSTATIC NOISE
ELECTRIC FIELD SPIKES
SEPARATRIX
NORTH LOBE
SOUTH LOBE
ENERGETIC ELECTRON STREAMS
ELECTRON HEAT FLUX
SUPRATHERMAL ION STREAMS
FAST-MODE WAVES
SLOW-MODE SHOCK
WHISTLER WAVES
JETTING PLASMA SHEET (OPEN)
ELECTRON PLASMA OSCILLATIONS
BROADBAND ELECTROSTATIC NOISE

FIG 7

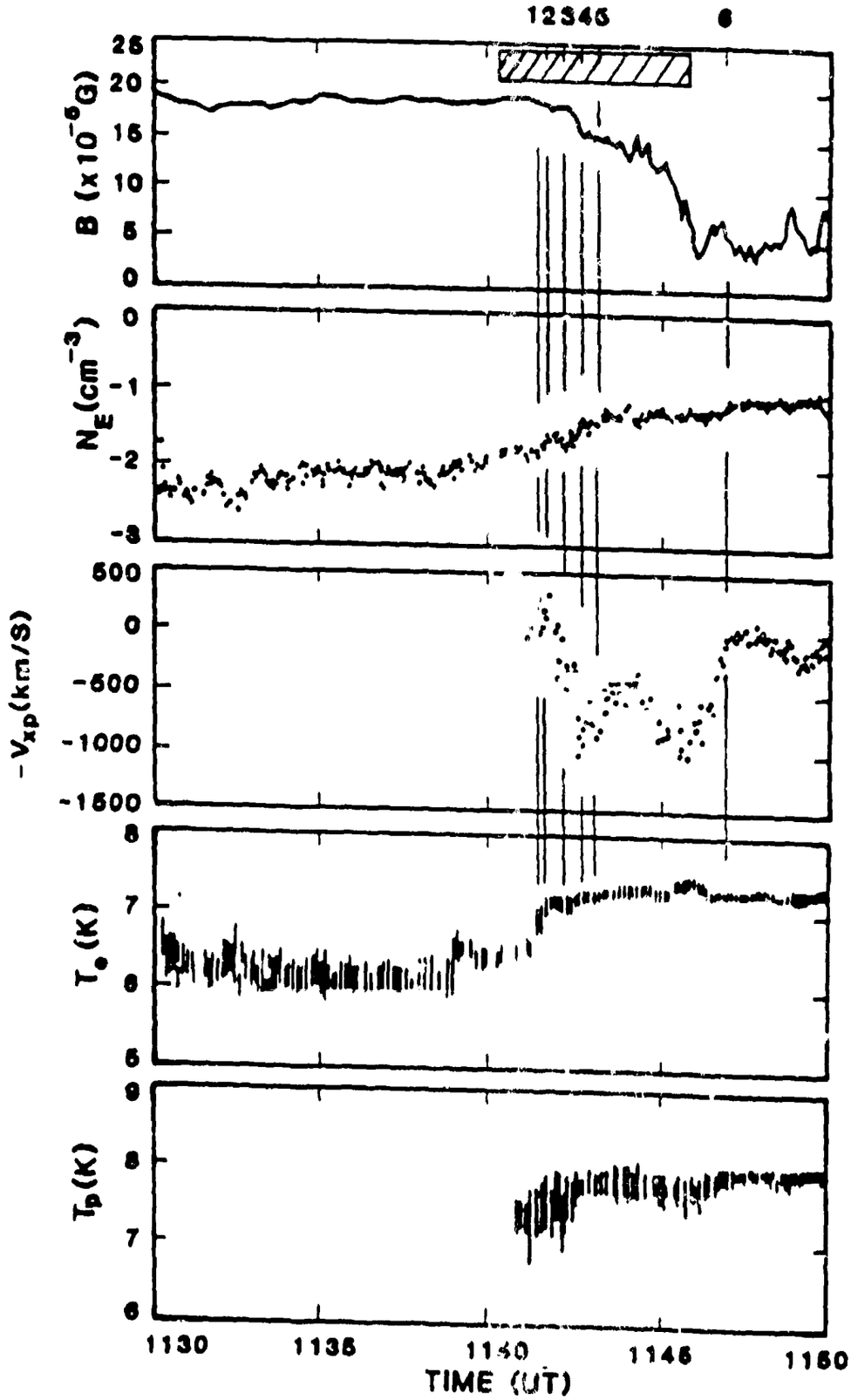
12345
B (x10^{-5}G)
25
20
15
10
5
0
N_E(cm^{-3})
0
-1
-2
-3
$-V_{xp}$(km/S)
500
0
-500
-1000
-1500
T_e(K)
8
7
6
T_p(K)
9
8
7
6
1130
1135
1140
1145
1150
TIME (UT)

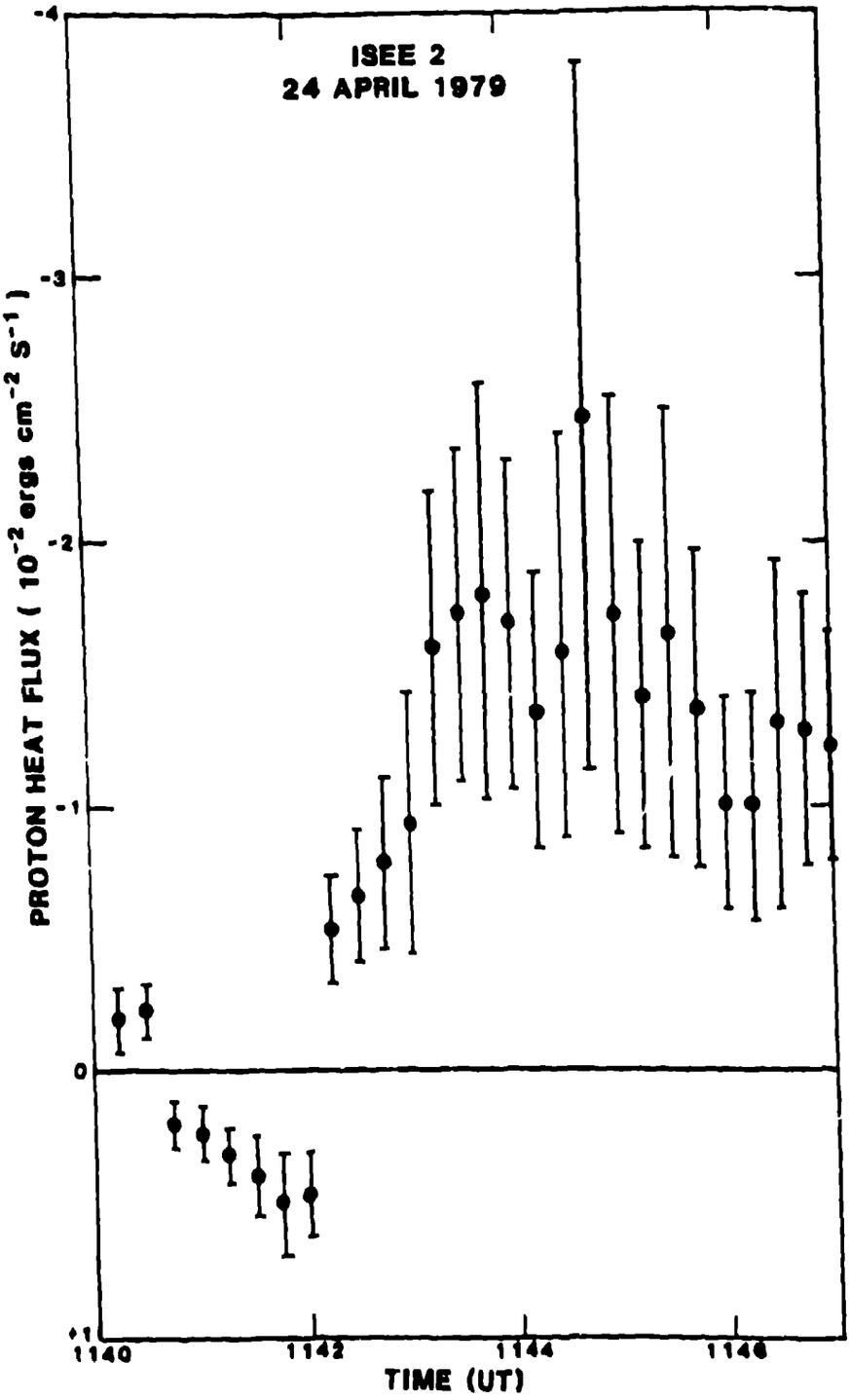
ISEE 2
24 APRIL 1979
PROTON HEAT FLUX (10^{-2} ergs cm^{-2} S^{-1})
-4
-3
-2
-1
0
+1
1140
1142
1144
1146
TIME (UT)

Fig 9

Fig 10

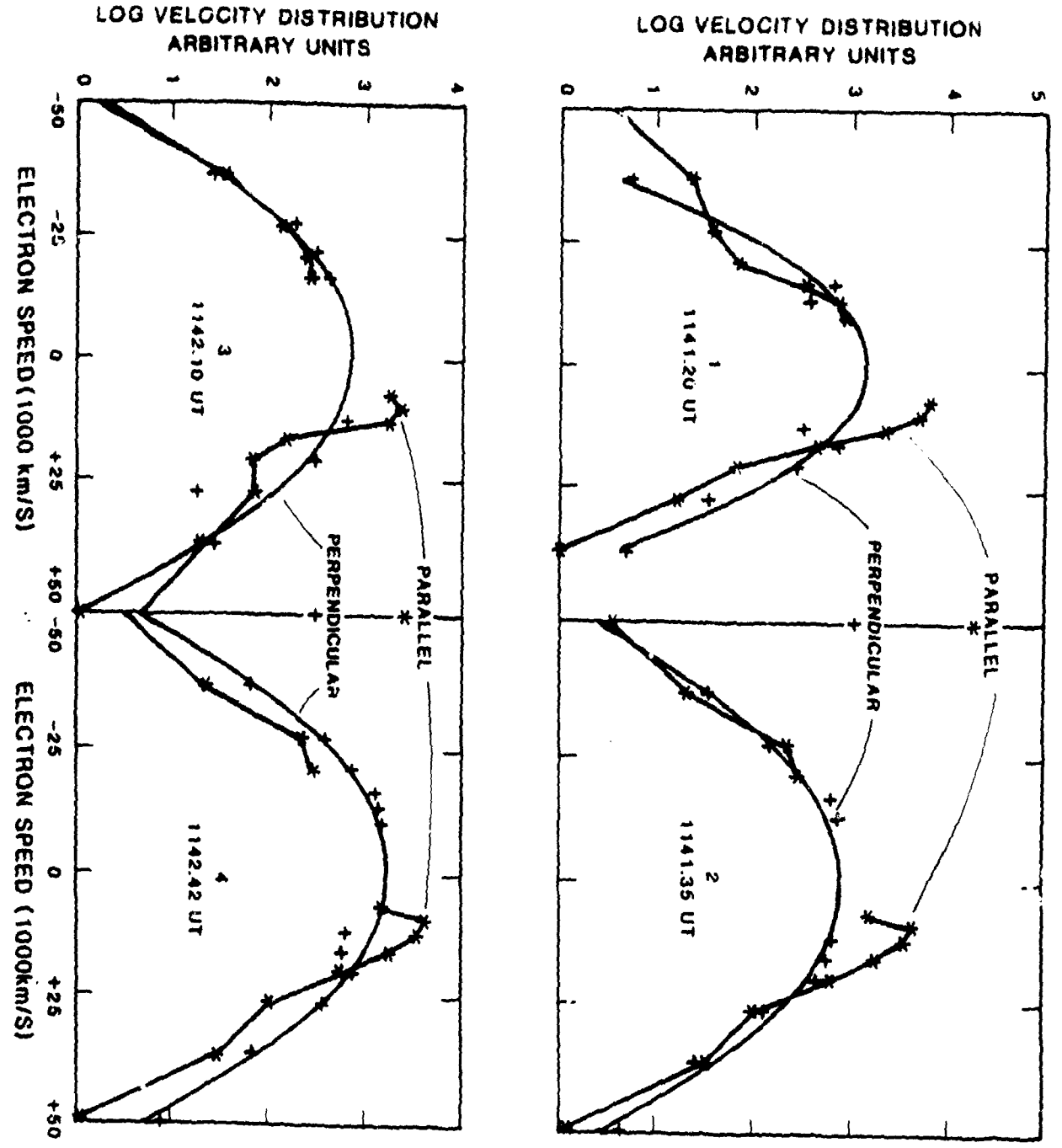
LOG VELOCITY DISTRIBUTION
ARBITRARY UNITS
0
1
2
3
4
5
1
1141.20 UT
2
1141.35 UT
PERPENDICULAR
PARALLEL
LOG VELOCITY DISTRIBUTION
ARBITRARY UNITS
0
1
2
3
4
3
1142.10 UT
4
1142.42 UT
PERPENDICULAR
PARALLEL
-50
-25
0
+25
+50
ELECTRON SPEED (1000 km/S)
ELECTRON SPEED (1000km/S)

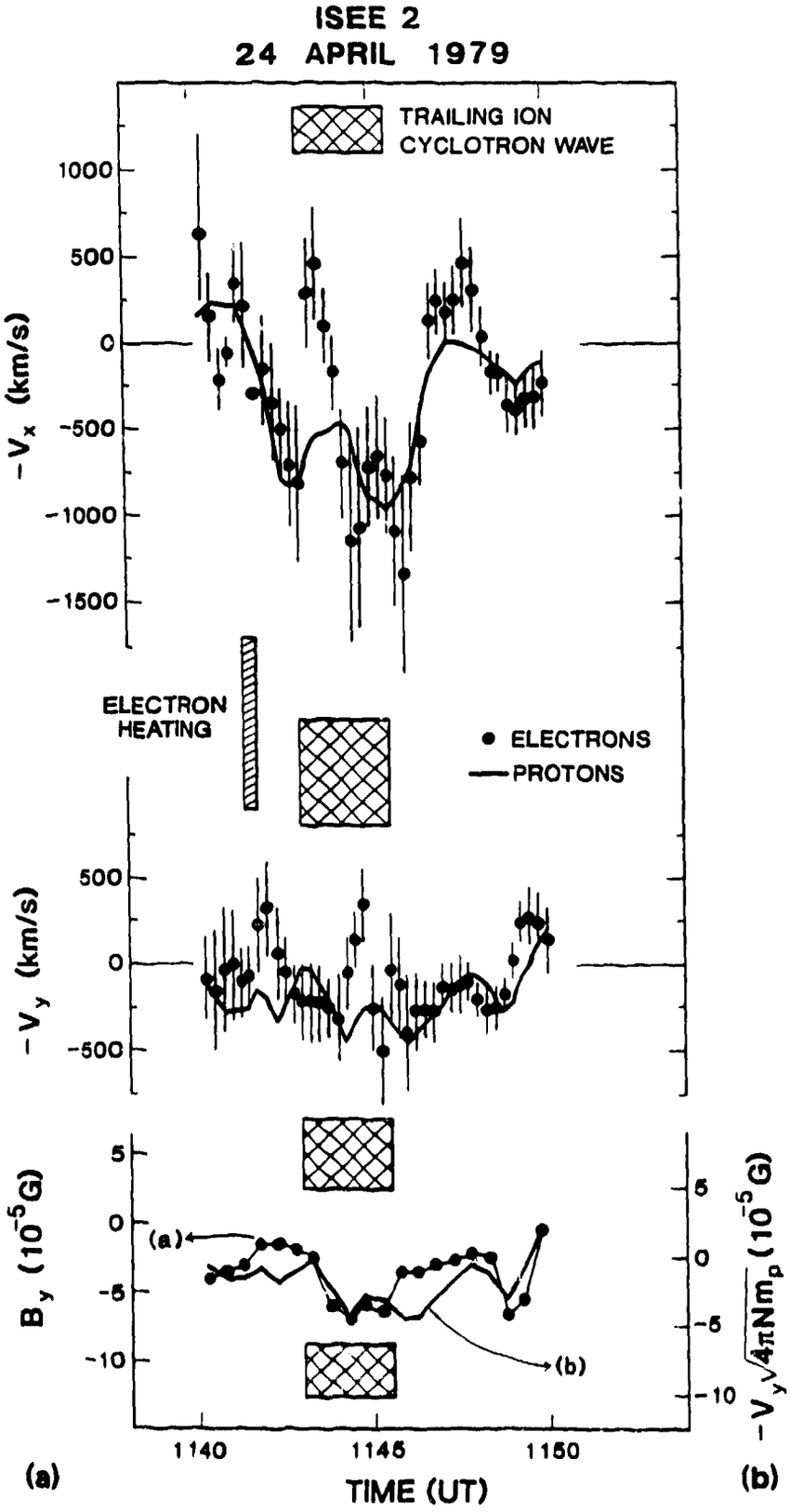
ISEE 2
24 APRIL 1979
TRAILING ION
CYCLOTRON WAVE
1000
500
0
-500
-1000
-1500
$-V_x$ (km/s)
ELECTRON
HEATING
ELECTRONS
PROTONS
500
0
-500
$-V_y$ (km/s)
5
0
-5
-10
B_y (10^{-5}G)
(a)
(b)
$-V_y\sqrt{4\pi Nm_p}$ (10^{-5}G)
1140
1145
1150
TIME (UT)
(a)
(b)

Fig 11

PLASMA SHEET CONFIGURATION CHANGES DURING A SUBSTORM

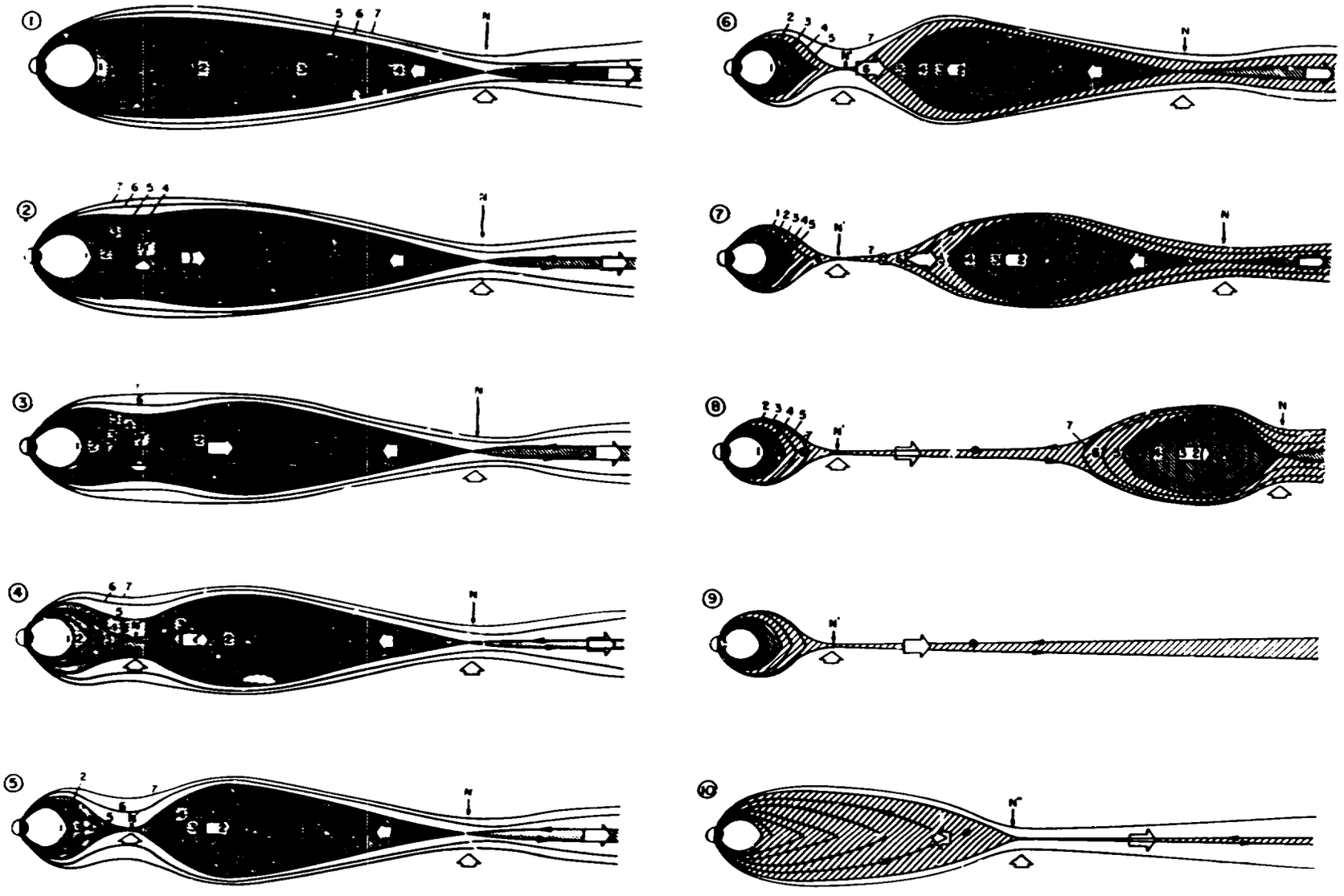

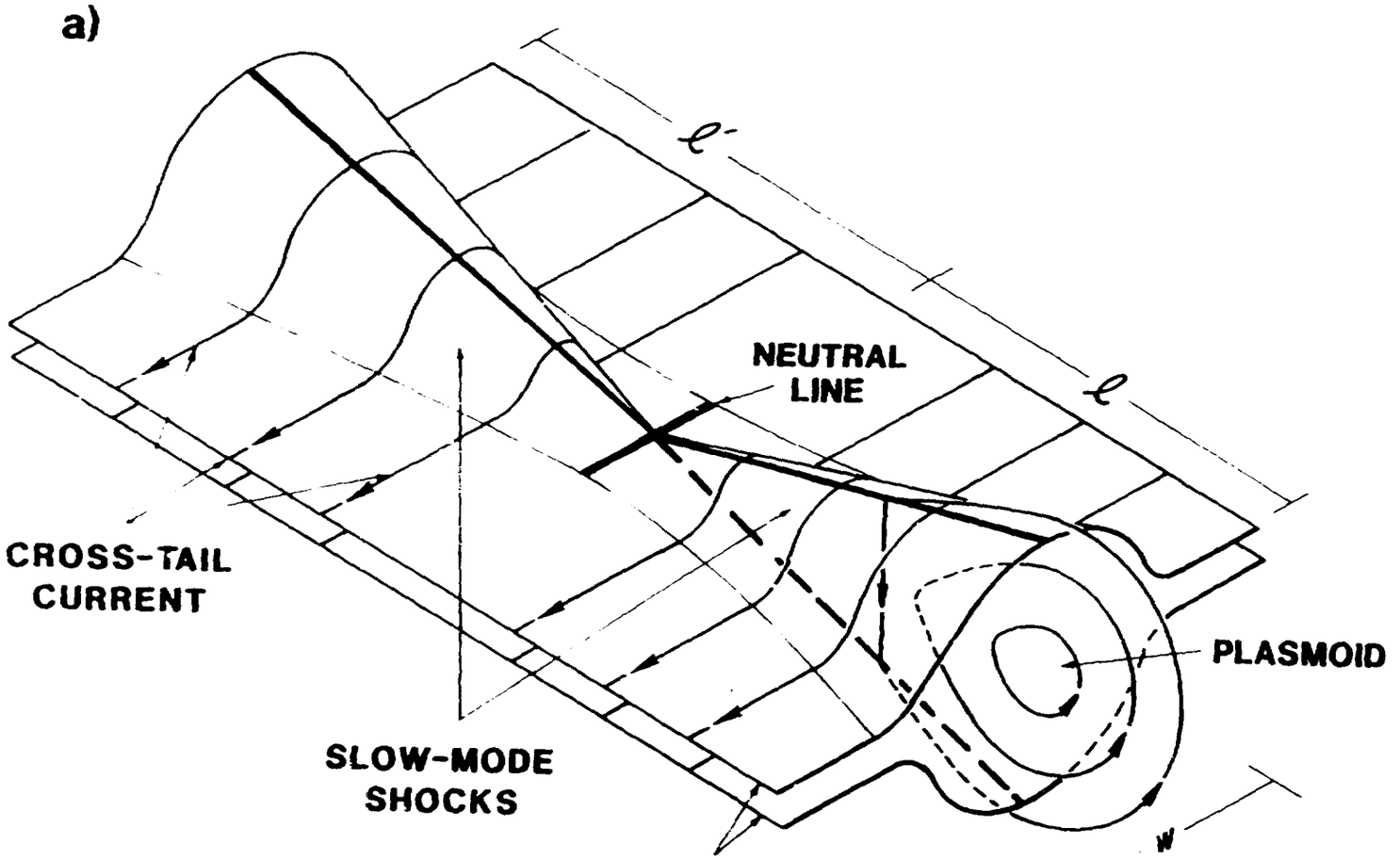
a)
NEUTRAL LINE
CROSS-TAIL CURRENT
SLOW-MODE SHOCKS
PLASMOID

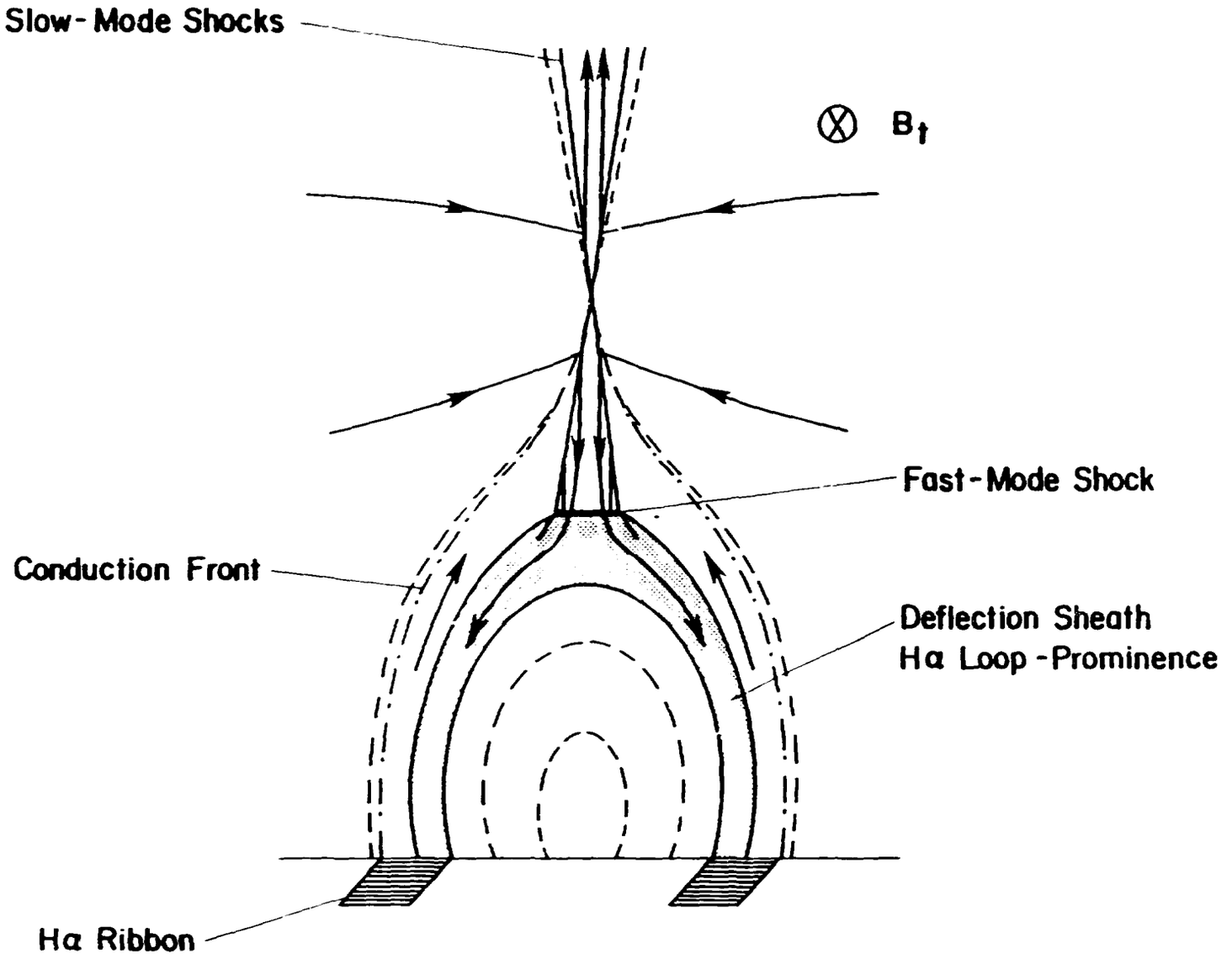

FIG. 1.—Schematic showing the MHD shocks generated by reconnection in a line-tied configuration. Dashed lines denote magnetic field lines, and dashed-dot lines, the conduction fronts generated by field annihilation at the slow-mode shocks. B_t is the transverse component of the magnetic field, out of the plane of the figure.